Investigation of Fibre Optics Instrumentation on Sprayed Concrete

By

Bonnie Leung Hiu Yu (T)

Fourth-year undergraduate project in
Group D, 2011/2012

Acknowledgements

It is a pleasure to thank those who made this project possible. First and foremost, I would like to express my sincerest attitude to my supervisor, Dr. Mohammed Elshafie for his patience, support and guidance throughout the course of my project. Without his insight, enthusiasm and motivation, I would not have been able to go through all the obstacles in completing this project.

I would also like to thank Masanari Nakashima, a PhD research student, for his help and intelligence ideas in preparing the experiments and data analysis. I am indebted to the technical team of the Structures Research Group, led by Mr. Martin Touhey, the chief technician, the carpenters of the Structures Workshop especially Mr. Steve Papworth and Mr. Alistair Ross for their opinions and help.

I hereby declare that, except where specifically indicated, the work submitted herein is my own original work.

Investigation of Fibre Optics Instrumentation on Sprayed Concrete

Bonnie Leung Hiu Yu (Trinity College)

Technical Abstract

This research investigates the use of Brillouin Optical Time-Domain Reflectometry (BOTDR), a distributed strain sensing technology, for monitoring the performance of structures made of Steel Fibre Reinforced Concrete (SFRC), widely known as strengthened sprayed concrete (SC). The BOTDR technology has the capability to measure continuous strains in structures, using the linear relationship between strain and Brillouin peak frequency shift. In real construction sites, information on ground conditions and loading is limited; therefore the behaviour of underground structures cannot be easily predicted. The BOTDR technology measures the complete strain profile within a structure by a single fibre optic cable embedded in it. This provides designers and infrastructure owners a better opportunity, compared to the conventional discrete vibrating wire strain gauge (VWSG) measurements, to understand the actual behaviour of their structures. This will result in more efficient designs for new structures and more effective maintenance strategies for existing ones.

In this project, the behaviour of a sprayed concrete beam (subjected to a four-point bending loading) and a sprayed concrete column (subjected to axial compression loading) were investigated in the CUED labs using BOTDR technology in addition to other conventional instrumentations. Comparing the measurements from BOTDR with other instrumentation will help significantly in appreciating the advantages and limitations of the technology when employed in real sprayed concrete structure, under more complicated loading conditions. There are implementation challenges that require careful consideration and planning. These include instruments configuration, installation methods, data processing and data interpretation. VWSG and demountable mechanical strain gauges (DEMEC gauges) were also

used in the lab tests and their measurements were studied at critical points for verification purposes.

The sprayed concrete beam and column were both prepared in the National Grid construction site in north London, They were then transported to CUED labs. Taking on board the lessons learnt from a similar project completed previously by other CUED researchers, the planning for casting SFRC beams on site including the formwork design and transportation methodology was significantly modified and improved. The sprayed concrete beam and column had a much higher quality than the previous project.

A uniaxial compression test (with loading and unloading cycles) on a 2.3 m SFRC column and a four-point bending test on 4.7 m SFRC beam were carried out. In the compression test, it was found that the VWSG gave higher strain measurements than the BOTDR. However, both showed similar trends of strain distribution along the column. In addition, the optical fibres measurements suggested a slight eccentricity in the axial loading. The results from the lab instrumentation compared well with empirical formula published in the literature.

For the four-point bending test, the sprayed concrete beam was tested in a horizontal plane and Teflon® sheets were put underneath the beam to reduce friction. The DEMEC gauges did not perform properly while the VWSG gave marginally higher strain readings, which led to a conclusion that the sprayed concrete has a much smaller Young's Modulus than predicted, while BOTDR gave a relatively closer estimation. The curvatures induced were studied where optical fibres pinpointed a local strain event successfully at the failure crack.

Results from both tests suggested that BOTDR technology is robust enough to be used in harsh environments (like sprayed concrete) and is capable of quantifying the overall performance of sprayed concrete structures to good degree of accuracy. The technology is also capable of identifying local strain concentrations in a precise manner.

Contents

1 Introduction

Performance monitoring is an important part of complex engineering constructions, to ensure health and safety, identify immediate dangers and evaluate critical design assumptions made based on uncertainties. Nowadays, engineers involved in designing tunnels using sprayed concrete, rely on conventional measurements from pressure cells and vibrating wire strain gauges (VWSG), which have plenty of associated problems. Their measurements give information at discrete locations, which makes it hard to understand the overall performance. They are highly affected by temperature changes, shrinkage, crimping and the installation process. Their life expectancies are usually short under harsh working environment, especially when withstanding the high pressure generated by the spraying of concrete. There is a need to implement a new monitoring technology that provides accurate information about the overall structural behaviour of sprayed concrete structures.

This research is based on a Crossrail construction site in the Liverpool Street station located near Finsbury Circus in central London, where series of cross passage tunnels are to be constructed, using sprayed concrete, between two existing platform tunnels. Breaking out for new tunnels is expected to cause significant stresses on the existing platform tunnels, both longitudinally and perpendicularly, that could be a cause for concern. With limited information on ground conditions and breakout effects, conservative assumptions and measures were made, including reinforcing the existing tunnels with additional concrete lining at the location of the cross passages. This results in significant time and cost implications and although it is generally felt that the reinforcing layer is not necessary, there is no strong evidence to show that the strains in the breakout region are insignificant.

An innovative monitoring technique that measures continuous strain profiles using optical fibres has been developed at the University of Cambridge. The Brillouin Optical Time-Domain

Reflectometry (BOTDR) has great advantages in quantifying the performance of underground concrete structure. This technique converts the change in density of the optical fibre cores, when experiencing bending, tension and compression, into strain measurements. The technology allows strains to be measured at every point along an optical cable for up to 10 km long with an accuracy of 30-40 $\mu\varepsilon$. Fibre optic cables can replace numerous of point sensors that would have been installed in collecting the same amount of information. It is a cost-effective monitoring solution when compared to VWSG. Reinforced optical fibres, moreover, survive under harsh working environment.

BOTDR offers very exciting potential in revealing the performance of underground structures as well as detecting local strain concentrations (cracks) at a relatively lower cost and a high degree of accuracy. Its practicality in sprayed concrete requires evaluation and hence is examined in this research. Simple laboratory tests on Steel Fibre Reinforced Concrete (SFRC) beams were conducted to understand the capability of the optical fibres to measure the strain distribution within the specimen. The findings from this study will pave the way for the optical fibre strain sensing technology to be used in the more complicated real life scenarios like the Liverpool Street station cross passages. This will provide a unique opportunity to measure the actual strains induced from the construction of the breakout holes in the platform tunnels and hence inform designers and decision makers on the relevance of the assumptions adopted in the design.

1.1 Scope and Objectives

The following describes the goals of this research:

1. To evaluate the capability of BOTDR technology in measuring axial and bending strains using simple SFRC structures (i.e. sprayed concrete beams and columns with no reinforcement bars) tested in the lab under controlled conditions.

2. To assess the practical issues and challenges which arise when employing BOTDR technology in sprayed concrete structures.
3. Understanding the issues related to data interpretation and data analysis of the optical fibre strain data, after the tests have been conducted.

2 Brillouin Optical Time Domain Reflectometry

2.1 Theory

BOTDR is a technology that relates strain to change in light property - the Brillouin peak. This distributed sensing system has been used in various projects for monitoring, such as piles foundations, soil nails and tunnel linings, by installing fibre optic cables along the areas of interest: attached to the surface or reinforcement bars embedded inside concrete structures. The major component of this technique is a standard fibre optic cable, which consists of three components: a core optical fibre, a glass cladding and external buffer as illustrated in Figure 2.1. The buffer serves as a protective layer whilst the cladding serves as a refractive medium of light.

The way the BOTDR technology works is straightforward. At either end of the optical fibre, a typical light pulse is launched. Scattering occurs due to the inhomogeneity of the refractive indexes between the core and the cladding. Backscattered light is then reflected back to the launch end and detected by an optical fibre strain analyser. A signal diagram is produced which records the power and wavelength of the backscattering light and identifies the characteristic peaks in corresponding locations in the fibre (Figure 2.1) .

The Brillouin peak is an important signature of backscattering light. The shifting of Brillouin peak, at the same location identified by the analyser, is proportionally dependent of temperature and strain due to the change in materials' intensity. This frequency shift is described as the Brillouin gain and is a vital element in this technology (Figure 2.3).

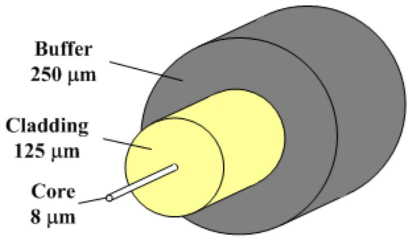

Figure 2.1 Single mode optical fibre (Mohamad 2008)

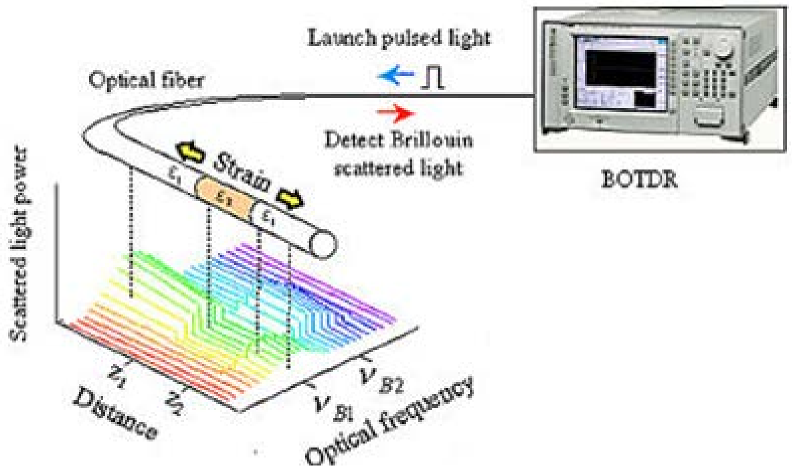

Figure 2.2 Peaks and locations identification by BOTDR

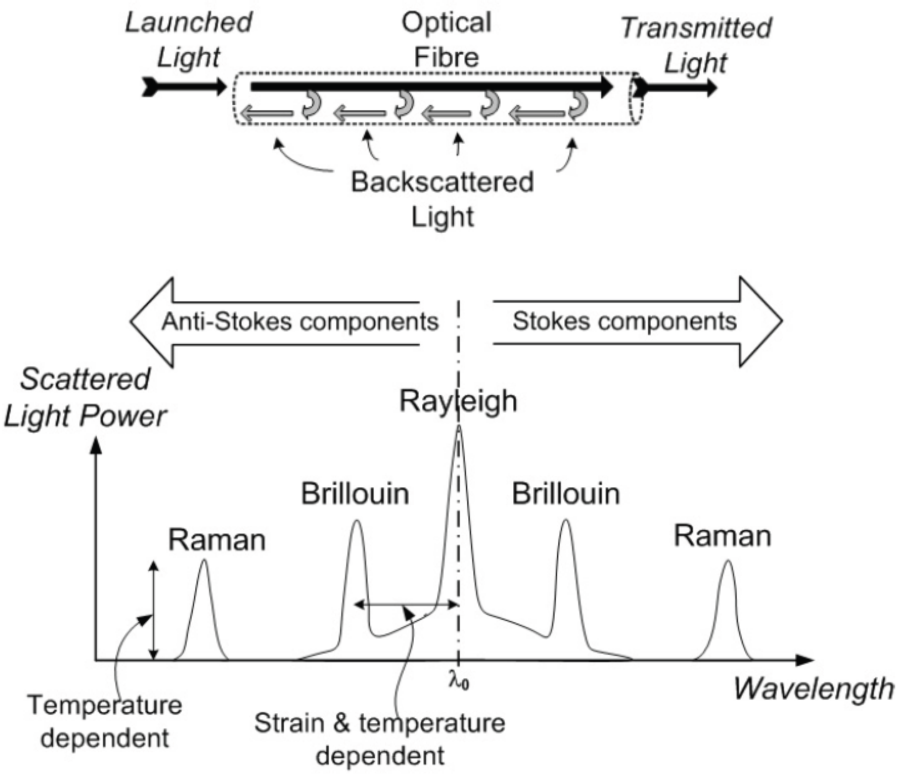

Figure 2.3 BOTDR theory on backscattering light (Mohamad 2008)

2.2 Equipment

2.2.1 BOTDR data analyser

AQ8603 Yokogawa Brillouin Optical Time Domain Reflectometry is the analyser used in this study. It is capable of measuring Brillouin frequency shift and displaying corresponding diagrams simultaneously whilst taking measurements. It has a high resolution with strain, which is averaged within ± 0.5 m, calculated at every 5 cm. The strain accuracy is in the range of ±0.0003 % to 0.0004 %. Only one end is required for operation, where information beyond a break point can be recovered by accessing the other end of the optical fibre. The cost of this piece of equipment is approximately £60,000 (2006).

2.2.2 Sensing fibres and cables

Optical fibres can be classified into single mode and multimode, whilst fibre optic cables can be categorised by their robustness and cost. Single mode optical fibres are typically used for monitoring to limit the amount of dispersion by having a small core. They are fragile and weak in bending but strong in tension.

Fibre optic cables ensure good condition and function of optical fibres. Fujikura reinforced ribbon cable (JBT-03813) is robust which comprises of 4 independent optical fibres and 2 steel wire reinforcement (Figure 2.5). Both sides of the cable are covered by nylon. The cost is £15.00/m (May 2012).

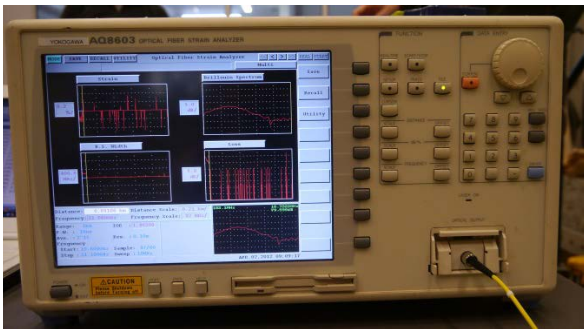

Figure 2.4 AQ8603 BOTDR analyser

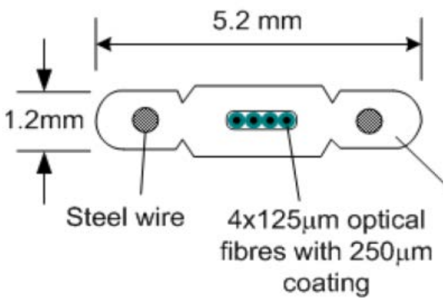

Figure 2.5 Fujikura reinforced ribbon cable (JBT-03813)

2.2.3 Temperature sensing cables

Loose tube cables such as Universal unitube cable, which consists of gel surrounding the optical fibres, stops the strains (from the matrix surrounding the cable) from being transferred to the optical cores. Temperature compensation is required in situations when where temperature changes are significant. In laboratory conditions where tests were conducted in a relatively short period of time, the strain measurements would not be significantly affected by temperature changes.

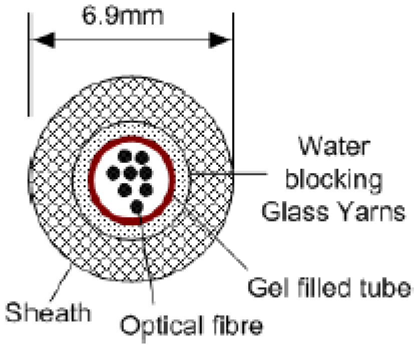

Figure 2.6 Universal unitube cable

2.3 Advantages and Disadvantages

Compared to the conventional VWSG, BOTDR technology is more beneficial as it produces continuous strain profile as opposed to discrete point measurements. It pinpoints the failure locations and leads to a better understanding in the overall structural behaviour. It can survive under harsh working conditions such as spraying of concrete and is not affected by electrical of magnetic interference.

However, the BOTDR analyser is expensive and delicate which increases the operational and maintenance cost. Moreover, the time required for light to be refracted causes construction delay.

3 Planning and preparation

3.1 Experimental tests

A uniaxial compression test for a sprayed concrete column and a four-point bending test for a sprayed concrete beam (both prepared in the National Grid site in north London) were tested in a controlled environment to investigate their behaviour using BOTDR technology. Other conventional instrumentation (VWSG, LVDT and DEMEC gauges) were used for comparison purposes.

3.2 Specimens design and considerations

Two specimens were designed to be tested under compression and bending. To maximize the number of data for analysis with higher accuracy, longer specimens were preferred. The length of specimen was restricted by the location of the bending test (with CUED) and the height of the hydraulic test frame (Amsler), in addition to the standard size available for the wooden boards for the formwork. It was decided that a 2.3 m column for compression and a 4.7 m beam for bending would be suitable. For the bending test, the loading points were applied at 0.85 m and 3.85 m to maximise the constant moment region in the middle.

The cross sectional area of both the column and beam were designed to be the same for the ease of manufacture (0.25 m x 0.25 m).

3.3 Formwork design

The aim for a formwork design is to produce desirable specimens for testing. A similar sprayed concrete test with a shorter beam was performed by CUED researchers in a previous project. The formwork design adopted in that project resulted in specimen with a poor quality. Improvements were adopted in the formwork design in this project to avoid those problems. .

Table 3-1 lists out the major failures in the previous design, their consequences and how the new formwork is enhanced. There were five additional features to this formwork, which is designed to hold 630 Kg of concrete beam:

1. Holes were drilled for the passage of VWSG cables and optical fibres.
2. Thin steel bars were added at an interval of 0.9 m (6 for the beam and 3 for the column) to guide the optical fibres and to provide structural support.
3. The formwork for the beam was designed in two pieces that can be joined together to make transportation easier.
4. Box panels were added to reinforce the connection between two parts of the formwork for the beam to prevent twisting.
5. Extra side supports constructed to add strength to the formwork.

Table 3-1 Formwork design improvement

Failures in previous design	Consequences	Improvements
Air pockets at the bottom of concrete beams caused by trapped air during casting	Concrete strength reduces.	Holes were drilled at the side of formwork to remove air during casting.
Beam too short	● Short constant moment section. ● BOTDR measurements average strain over 1m. Therefore short constant moment sections will introduce uncertainty in interpretation.	Longer beam length of 4.7 m (Distance between two loading point is 3 m)
No backing-up devices	Cannot verify BOTDR measurements.	DEMEC & Strain gauges embedded inside of the concrete as back-ups.

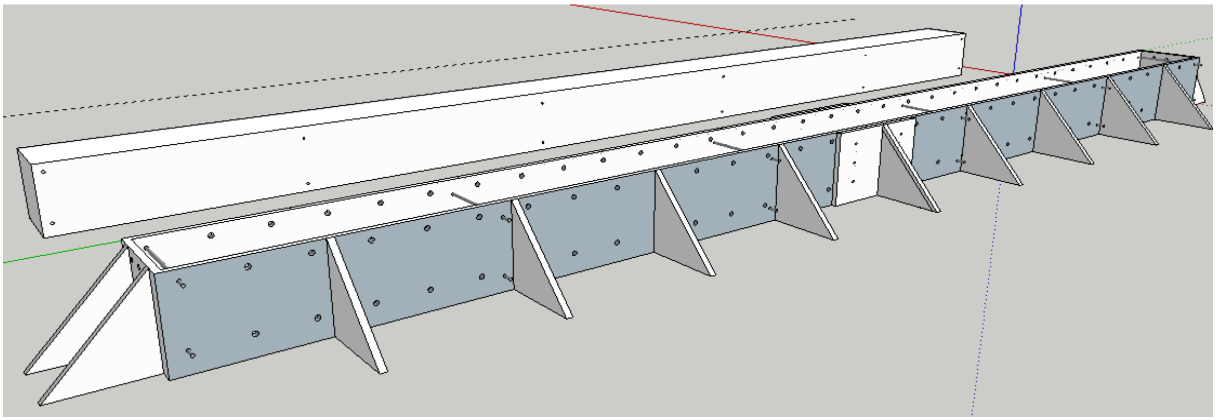

Figure 3.1   Initial design for the frame work

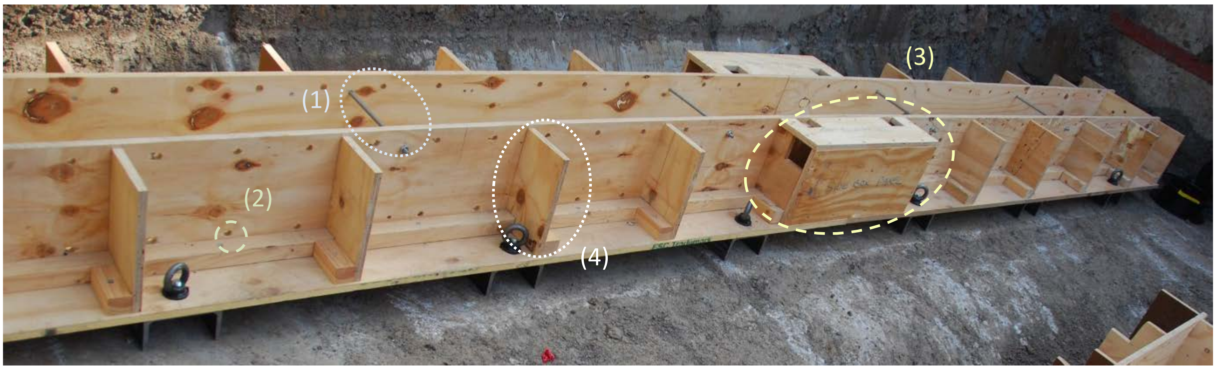

Figure 3.2   Actual formwork

(1) Holes reserved for steel bars, (2) Air holes, (3) Box panel, (3) One of the extra supports

3.4 Lifting design and arrangement

Due to lack of reinforcement in the concrete, careful lifting considerations were taken to prevent excessive deflection and twisting of the formwork with sprayed concrete at early stages after casting. This design was prepared with the assistance of a specialised lifting company, which verified the design and provided the necessary paperwork. The beam is lifted from the bottom using six channel sections as seen in Figure 3-3. The channel sections have eyebolts at the two ends (Figure 3-4) at which the lifting chains were connected. The lifting chains were then fixed to the lifting beams at three locations. The beam is lifted from a single point in the middle. A drawing of the lifting design was produced and corresponding parts were built with the help of the carpenters in CUED departmental workshop.

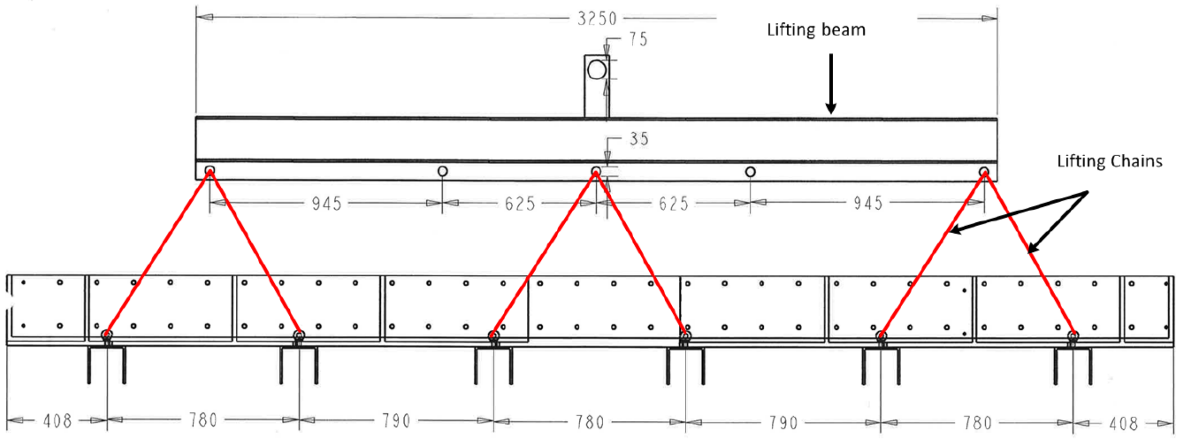

Figure 3.3 Lifting arrangement with specialist lifting rig

Figure 3.4 Eyebolt and lifting chain with part of the support removed to allow full chain stretching.

3.5 Instrumentation configurations

Optical fibres and VWSGs were embedded in the concrete in configurations shown in Figure 3.5. The arrangement in bending allows measurements to be taken in the compression and tension zones for comparisons. Since the column under uniaxial compression is expected to have constant strain throughout, for the ease of installation, instruments were place at one side of the column, which corresponds to the lower zone of the beam cross-section.

The fibres were installed throughout the specimen length, while the strain gauges were placed at the constant moment zone. (Figure 3.7)

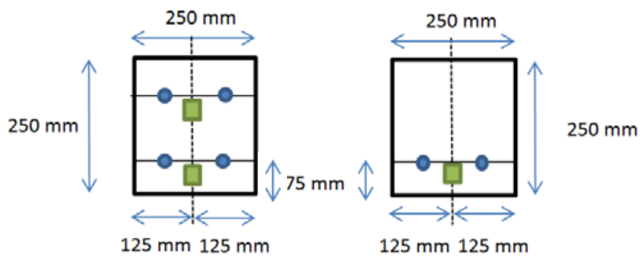

Figure 3.5 Instrumentation configurations at the cross-sections (Left: beam, Right: column)

3.6 Instruments Protection

Optical fibres are protected by a plastic coating which was considered to be dependable, but VWSGs are very fragile and required further protection. The sensitive part of the strain gauge was protected by bubble wrap, whilst the exposed cable was wrapped with duct tape. A red label was attached later that defines the upward-facing surface as indicated in the Model 4200 strain gauges manual.

Figure 3.6 Protected VWSG

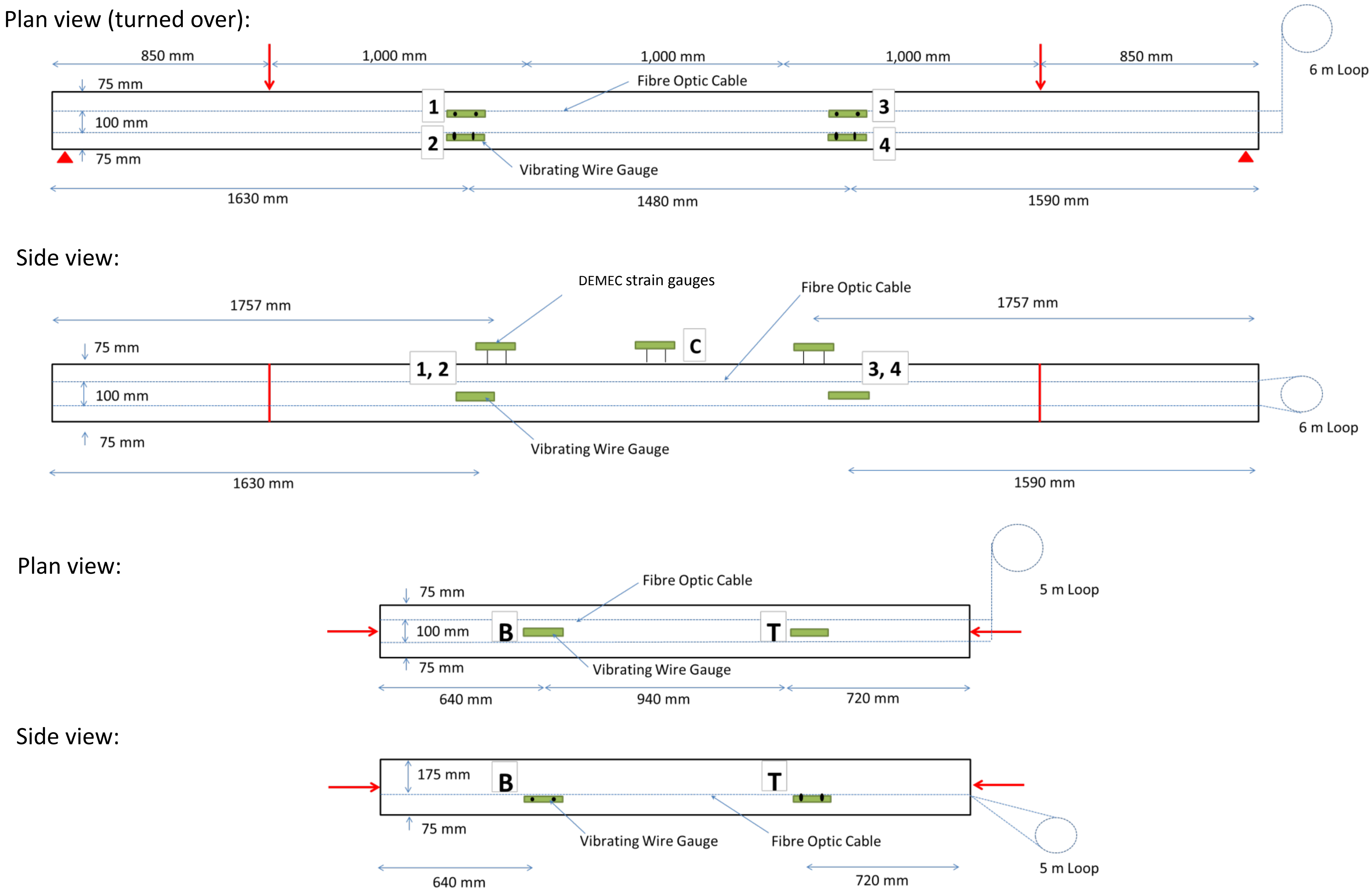

Figure 3.7 Instrumentation Configurations at plan and side views (Top: beam, Bottom: column), amended version after actual installation.

3.7 Theoretical Predictions

3.7.1 Steel Fibre Reinforced Concrete Weight

The concrete mix used in the test beam and column was provided by Hanson Concrete (UK). Table 3-2 shows the details of the mix.

Table 3-2 Steel Fibre Reinforced Concrete mix

Cemi	450 kg/m3
Limestone	450 kg/m3
Sand Marine	1150 kg/m3
Plasticiser	0.7 L/100Kg
Fibre poly/plastic	0.9 kg/m3
Dramix® Fibres steel (Vf.=1%)	35 kg/m3
Retarder	4 L/m3
free water	187 kg/m3

The steel fibres used were Dramix®, manufactured by Bekaert. They were 35 mm in length, 0.55 mm in diameter with an aspect ratio of 65 and tensile strength of 1300 MPa and fulfil the requirements for both ASTM A820 and ISO 9001.

The predicted concrete unit weight was calculated by adding up the weights of materials in one metre cube of concrete mix with a water to cement ratio of 0.41. It was estimated at about 2273 Kg/m^3. This is within the typical SFRC density range from 2250 Kg/m^3 to 2400 Kg/m^3.

3.7.2 Steel Fibre Reinforced Concrete Strength

The bending test and the compression test were conducted 18 days and 29 days after casting respectively, the strengths of SFRC in testing were predicted based on its 24-hour strength. Two concrete strength tests were carried out by the site engineers 24 hours after casting. The cylindrical concrete strength measured was 25 MPa. With the presence of steel fibres, the compressive strength of concrete is increased by up to 15% (Labib, W., Eden, N. 2006).

However, Dramix® fibres do not enhance the compressive strength as much as other shapes of fibre (crimped, paddled, and irregular), however they cause a significant increase in the peak strain. (Dhakal, R.P., Wang, C., Mander, J.B. 2005)

The compressive strength of SFRC depends on the fibre quality and volumetric ratio V_f. It also has a close relation to the corresponding plain concrete compressive strength. Equation (3-1) estimates the SFRC compressive strength according to the factors mentioned:

$$\frac{f_{peak}}{f'_c} = 1 + 20\alpha_f V_f$$

(3-1)

(Dhakal, R.P., Wang, C., Mander, J.B. 2005)

where $\frac{f_{peak}}{f'_c}$ = normalised compressive strength which equals to the ratio of SFRC cylindrical compressive strength and plain concrete cylindrical compressive strength

α_f = experimental constant (0.5 for SFRC concrete with 1% Dramix® fibres)

With the volumetric ratio of 1%, the corresponding plain cylindrical compressive strength after 24 hour is 22.7 MPa, which matches with the strength of plain concrete at 0.4 W/C after 1 day in Figure 3.8. It is reasonably close to the actual W/C ratio of the specimen, which is 0.41. The curve gives a cylindrical compressive strength of plain concrete after 18 days of 50 MPa. Equation (3-1) predicts the SFRC cylindrical compressive strength to be approximately 55 MPa. This strength is converted to cubic compressive strength of 61.5 MPa by Equation (3-2). Similarly after 29 days, the cubic compressive strength is predicted to be 65.2 MPa.

$$\frac{F_{cyl}}{0.8^{0.5}} = F_{cu}$$

(3-2)

where F_{cyl} = cylindrical compressive strength (MPa)

F_{cu} = cubic compressive strength (MPa)

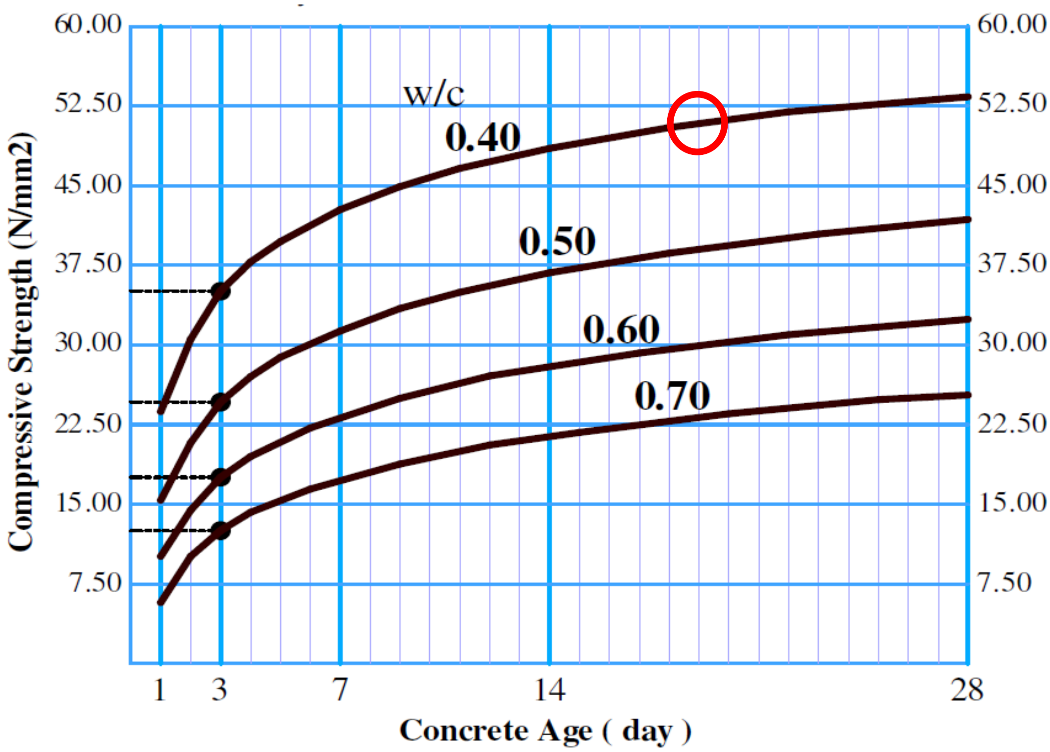

Figure 3.8 Prediction of compressive strength of plain concrete at various water cement ratio using neural networks. (Labib, W., Eden, N. 2006)

3.7.3 Steel Fibre Reinforced Concrete Stiffness

The stiffness of concrete is quantified by its Modulus of elasticity (Young's Modulus), E. It is predicted with the use of cubic compressive strength estimated in the previous section. According to the CEB-FIP Model Code 1990 (1993) (Equation (3-3)), The Modulus for SFRC 18 days and 29 days after casting are approximated to be 39.4 GPa and 40.2GPa respectively. The Modulus is roughly 620 to 640 times its strength.

$$E_{ci} = 21500 \left[\frac{f_{cm}}{10}\right]^{\frac{1}{3}}$$

(3-3)

Where E_{ci} = tangent modulus of elasticity (MPa)

f_{cm} = uniaxial compressive compression strength (MPa)

An evaluation of modulus of elasticity for SFRC was published (Jo, B.W., Shon, Y.H., Kim, Y.J. 2001) and concluded that the estimation equation for concrete with compressive strength less than 60 MPa should be:

$$E_c = 6191\sqrt{f_c} - 13540 - 2.4\, Isf$$

(3-4)

(Jo, B.W., Shon, Y.H., Kim, Y.J. 2001)

where E_c = modulus of elasticity (MPa)

f_c = cubic compressive strength (MPa)

Isf = steel fibre index which equals to volumetric ratio of steel fibre x steel fibre aspect ratio

With steel fibre aspect ratio is 65, $Isf = 0.0065$, the modulus of elasticity of the SFRC is estimated to be 34.0 GPa, slightly smaller than the figure predicted by Equation (3-3).

3.7.4 Steel Fibre Reinforced Concrete Tension

Reinforced Concrete normally has tensile strength 8-15 % of compressive strength (MacGregor, J. G. , Wight, J 1997), therefore for this specific SFRC, the tensile strength is predicted to be within the range of 4.72 MPa to 8.85 MPa.

Equation (3-5) for SFRC tensile strength prediction is derived by a statistical approach. It predicts the tensile strength to be 4.72MPa, which is the minimum within the range.

$$\sigma_{st} = 0.9508\sigma_{mt} \times V_f \times P \times e^{QA} \quad (3\text{-}5)$$

$$\mathrm{P} = 1.29276 - 0.337235 \quad (3\text{-}6)$$

$$\mathrm{Q} = -0.08029 + 0.01255V_f \quad (3\text{-}7)$$

(Shende, A.E., Pande, A.M. 2011)

where σ_{st} = SFRC tensile strength (MPa)

σ_{mt} = plain concrete tensile strength (MPa)

V_f = volumetric ratio of steel fibre

A = aspect ratio of steel fibre

3.7.5 Maximum compressive loading

The size of the SFRC for the column compression test is 0.25 m x 0.25 m x 2.3 m. Prediction was made assuming the column undergoes pure vertical uniaxial loading with no eccentric loading. Failure load based on compressive strength is evaluated in Equation (3-8), the maximum load allowed is 3687.5 kN:

$$\mathrm{F} = f_{cu} \times A \quad (3\text{-}8)$$

Where f_{cu} = cubic compressive strength (MPa)

A = cross sectional area (mm^2)

Buckling load is evaluated in Equation (3-9)

. The buckling loading is 23600 kN which is bigger than 3687.5 kN. Therefore the critical failure load is 3687.5 kN.

$$P_b = \frac{\pi^2 \cdot E \cdot I}{(k \cdot L)^2} \quad (3\text{-}9)$$

where E = modulus of elasticity

I = Geometric moment of inertia = $\frac{bh^3}{12}$

k = 1 for buckling coefficient for both ends pinne

L = total length

3.7.6 Compressive stress-strain relation

Stress-strain relation are highly affected by the types of fibres, including shape, aspect ratio A and volumetric ratio V_f. Predictions were made using various theories that focused on the effect of Dramix® fibres in concrete with compressive strength in the range of 35 MPa to 85 MPa. (Carreira, D. J. , Chu, K. M 1985)and (Soroushian, P. , Lee, C. D. 1989) were two of the earliest studies that evaluated stress-strain relation in SFRC, however their equations only depend on V_f and A which may not be sufficient in reflecting the effect induced by the shape of fibres. More experimental works on the impact of fibres' shape were conducted later where three focused mainly on Dramix® fibres, these are (Ezeldin, A.S., Balaguru, P.N. 1992), (Barros, J. A. O., Figueiras, J. A 2005) and (Dhakal, R.P., Wang, C., Mander, J.B. 2005). They came up with equations that were specially set up for Dramix® fibres with volumetric ratio from 0.75 % to 1 %.

All theories give rather similar predictions in stress-strain relation (Figure 3.9). These predictions are discussed further in Section 6 Results and Observation.

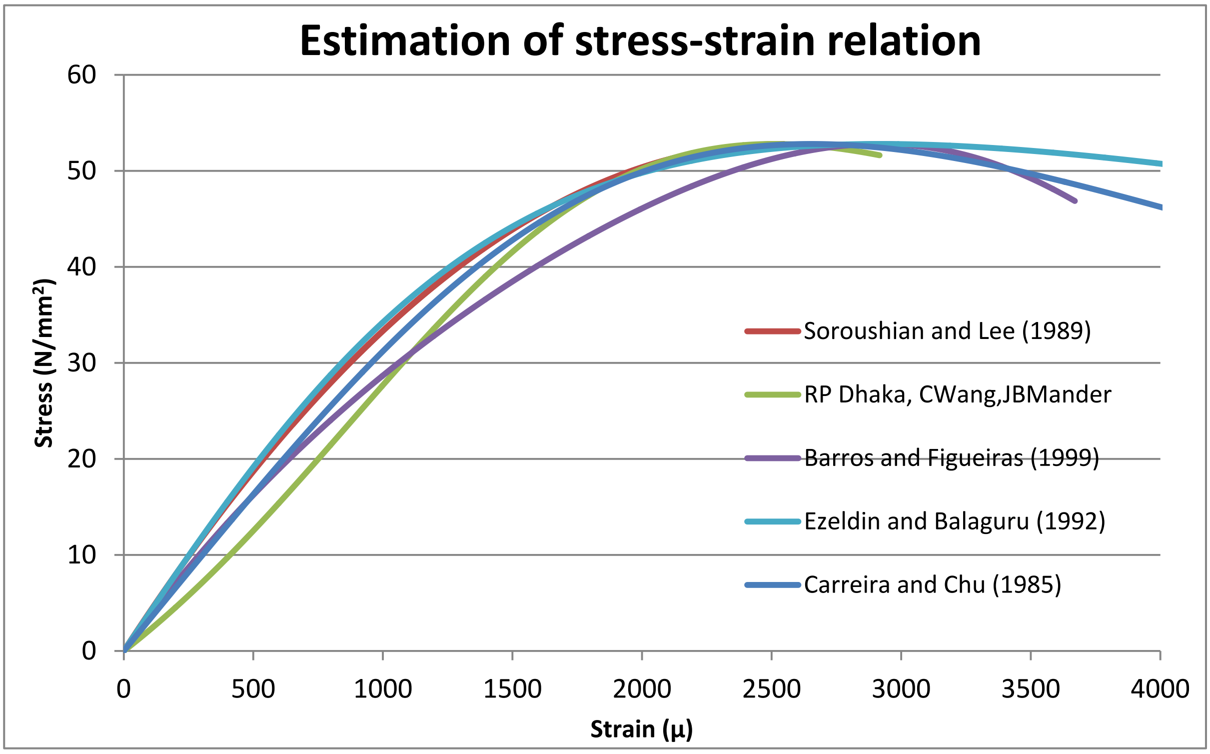

Figure 3.9 Estimation of stress strain curve by various theories

3.7.7 Maximum deflection in 4-point bending

The size of the SFRC for the beam-bending test is 0.25 m x 0.25 m x 4.7 m. It is assumed that self-weight can be ignored. The only force exerted on the beam would be the two point loads acting 0.85 m from each end. The maximum deflection is judged by the tensile strength of SFRC. 4.72 MPa was adopted because it is critical.

Tensile strength is defined as ratio of maximum moment and the section modulus:

$$\sigma_t = \frac{M}{Z}$$

(3-10)

where $M = \frac{P}{2} \times 0.85 = 0.425\text{P}$

$$Z = \frac{B \cdot H^2}{6} = \frac{0.25 \cdot 0.25^2}{6} = 0.0026$$

So, the maximum loading at each point = P/2 = 28.88 kN/2 = 14.44 kN

Maximum deflection at the centre can be estimated by:

$$\delta = \frac{0.85P}{48EI} \cdot (3L^2 - 4(0.85^2))$$

(3-11)

With the critical Young's modulus of SFRC predicted as 34 GPa, the maximum deflection expected at the centre of beam was 2.93 mm. Since the self-weight of concrete was 1/4 of the maximum loading, the assumption of neglecting self-weight should not be considered. A new testing mechanism was hence introduced: testing the beam in a horizontal plane (sideway bending). This allows loads to be applied horizontally to the beam. Under this set up, self-weight does not affect the overall deflection behaviour, given that the friction along the side of the beam is minimal. The beam can hold more additional load, therefore more data can be collected for analysis. Teflon® sheets were put underneath the beam to reduce friction. Validation tests were carried out to confirm whether it was effective or not. This is discussed in the next section

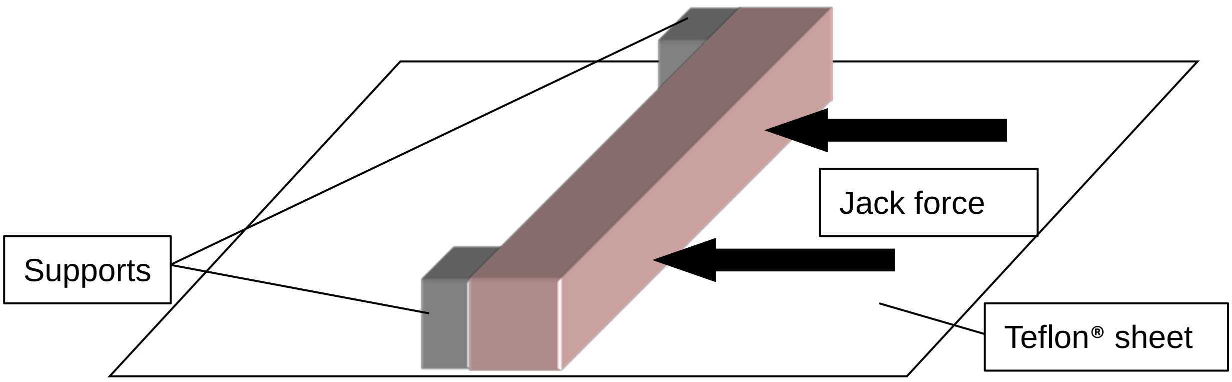

Figure 3.10 Sideway-bending test mechanism

3.7.8 Teflon® validation test

Since a sideway bending mechanism was adopted, friction effect along the length of the beam has to be reduced to maintain the feature of constant moment between the loading points for BOTDR verification. Teflon® sheets are common materials used in the industry to reduce surface friction. According to the manufacturer specification, the friction coefficient of the Teflon® sheet should be approximately 0.04. Validation tests were carried out to evaluate this friction coefficient with two sets of Teflon® sheets: 0.5 mm Teflon® sheet pair with PTFE sprayed in between and 3 mm Teflon® sheet pair with no PTFE sprayed.

The experiment involved a concrete weight 111 kg (0.5 m x 0.5 m x 0.2 m), two linear variable differential transducers (LVDT), a mechanical screw jack with ground supports, a wooden plate and a pair of Teflon® sheets. Two LVDTs monitored the movement of concrete block, whilst the wooden plate ensured even distribution of load to the surface of the block.

The performances of these combinations were tested under two different loadings for consistency. These results are given in Table 3-3. The friction coefficient of the 0.5 mm Teflon® sheet pair with PTFE sprayed was at the range of 0.081 – 0.083 while that of the 3 mm Teflon® sheet pair was at the range of 0.090 – 0.095. Although the 0.5 mm Teflon® sheet pair was more efficient in reducing friction, it was damaged at the end of the test.

The 3 mm Teflon® sheet pair can reduce friction with a similar efficiency but was less damaged; hence it was selected for the bending test.

Table 3-3 Teflon® tests results

Type	Weight (Kg)	Load applied to move (Kg)	Friction coefficient
0.5 mm sheet pair with PTFE sprayed	111	9	0.081
	180	15	0.083
3 mm sheet pair	111	10.5	0.095
	190	17	0.090

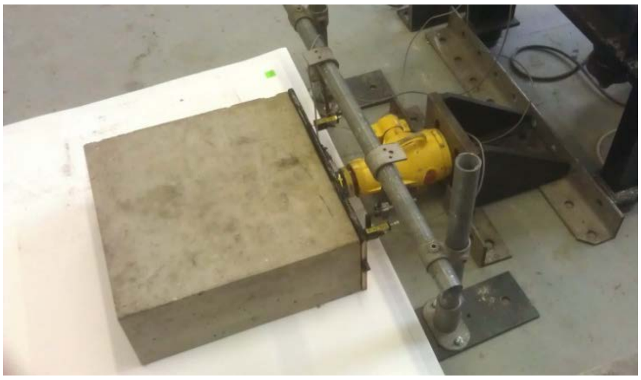

Figure 3.11 Teflon® sheet test set up

4 Site Work

4.1 Casting and Installation Procedures

The procedure for casting and installation of the instrumentation for both the beam and the column were very similar. There were a total of three layers of sprayed concrete required for the beam, whilst only two for the column. Two strings of fibre optic cables were embedded each layer and two VWSGs were installed at locations as shown in Figure 4.1. Pre-tension was required for the fibre optic cables to produce a strain signature to identifies its location within the specimen when reading from the data trace.

An initial layer of 75 mm of concrete was sprayed for the beam specimen. The fibre optic cables were then threaded through the predrilled holes at the ends and tightened using a pair of Fujikura pre-tensioning clamps. A pre-tension strain value of 2000-3000 με was imposed in the fibre optic cables manually. The VWSGs were laid on the concrete surface with red label facing upwards and held with two pair of nails. The VWSG cables were then guided out of the formwork through the access holes and were temporarily protected in the box panel. Another layer of sprayed concrete of 100 mm was sprayed where second set of instrumentations were installed with the first layer fibre optic cable looped back. A final layer of 75 mm was applied up to the top of formwork.

An initial layer of 75 mm of concrete was sprayed for the column specimen; with the instruments installed and pre-strained between another layer of concrete of 175 mm.

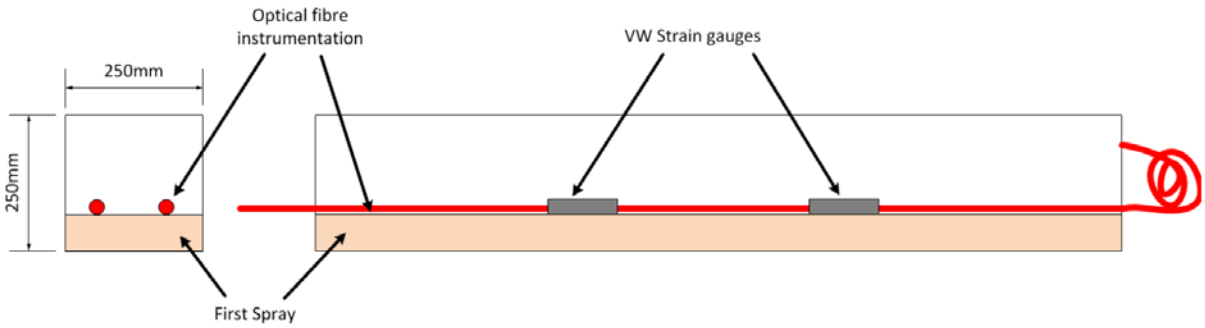

Figure 4.1 First layer of spraying and instrumentation installation

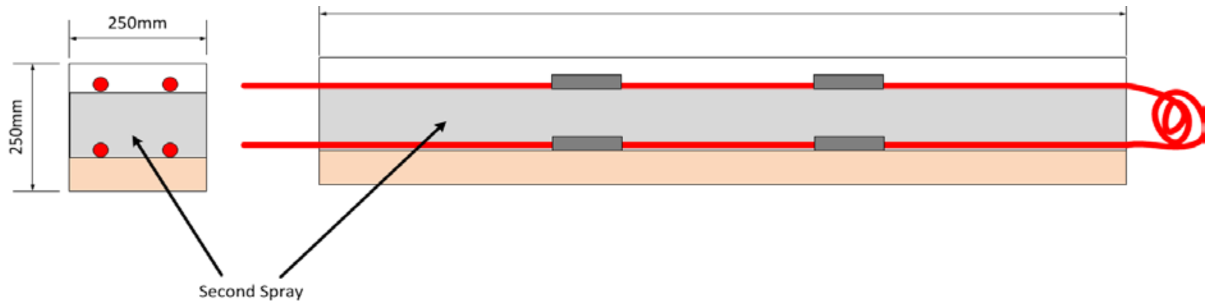

Figure 4.2 Second layer of spraying and instrumentation installation

Figure 4.3 The layout of instrumentations (Left: beam, Right: column)

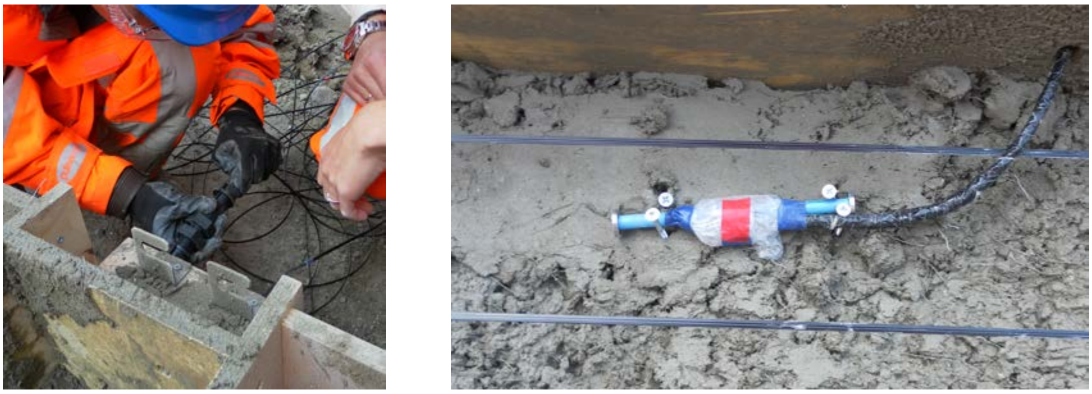

Figure 4.4 Instruments installation

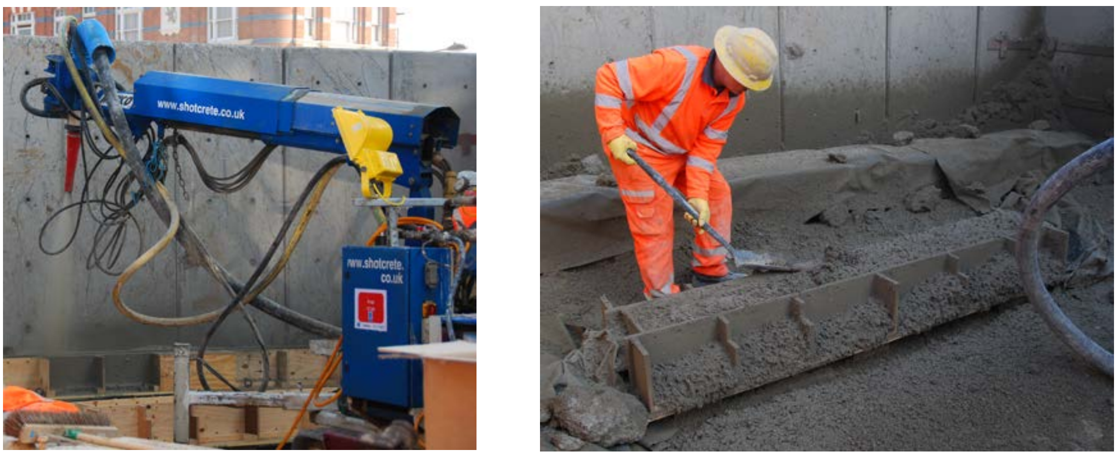

Figure 4.5 Spraying and finishing

4.2 Splicing techniques

Splicing is required for joining the fibre optic cables to the connecter for the strain analyser. Fibre optics is protected by at least two layers of coating: the plastic cladding and the external buffer as shown in Figure 4.6, they were removed using primary and secondary coating strippers. The fibre was then cleaned with alcohol, encased using a FP-3 splice protector and secured in a holder. This was then put in a high precision cleaver where the fibre was cut into suitable length for splicing (Figure 4.7). The same procedures were applied to the connector fibre. A splicing machine, Fujikura FSM 30R Fusion Splicer, was used as illustrated in Figure 4.8. It required approximately one minute for the process to be completed. The weak connected fibres were then taken out and sealed using the previously installed splice protector and were heat treated for approximately four to five minutes. The whole structure was then protected by two layers of plastic tapes (Figure 4.9).

The splicing process requires high precision which may be impractical outside laboratory condition.

Figure 4.6 Removal of protective layers

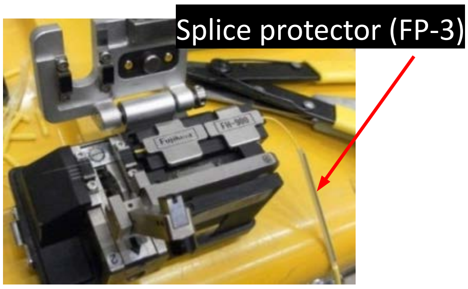

Figure 4.7 Optical fibre in cleaver

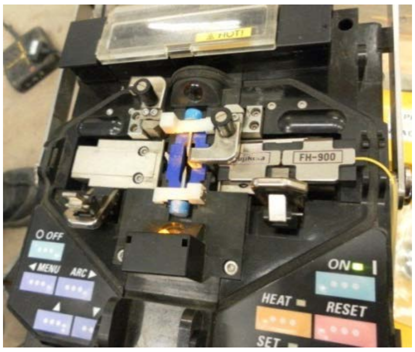

Figure 4.8 Fujikura FSM 30R Fusion Splicer

Figure 4.9 Plastic protectors

4.3 Test specimens

There were significant improvements in the quality of specimen with the use of new formwork as illustrated in Figure 4.10. The specimen surface was smooth with just a few blemishes at the corners. Vibrator was not used for sprayed concrete due to quick setting time.

Figure 4.10 Comparison of the quality of specimen (Left: Previous project, Right: this project)

The embedded fibre optic cables were checked using optical fibre strain analyser upon arrival to ensure they are in good condition. The pair of fibre optic cables was spliced together so that a full set of measurement can be recorded simultaneously by the analyser. A break in the optical fibre was detected near the loop end of the column. It was difficult to locate the exact location of failure as BOTDR can only measure the average strain within ± 0.5 m. When the clamps for the column were removed, a kink was found at the end of the column. As splicing was not possible at such location, two independent measurements, from the two ends of the cable, were taken to obtain all measurement from the column.

VWSGs were checked with electricity connected to the read-out box. It confirmed that the two strain gauges in column were in good condition; however one of the four strain gauges in the beam was out of order. It may be damaged under the harsh spraying conditions on site.

5 Experimental Work

Uniaxial compression test and the four-point bending test were performed. Although these might be different from the complicated real life site conditions, they are very useful in providing a well-controlled testing condition.

5.1 Compression

5.1.1 Set up

The Amsler is a servo-controlled hydraulic machine which has a load capacity of 5000 kN. It was used to apply axial compression loads onto the concrete column as illustrated in Figure 5.1. The loading machine comprises a hydraulic jack situated at the bottom platen while the load is carried to the column towards the top platen. A bearing system is situated at the top platen, which allows rotation for self-adjustment, a load of more than 50 kN is suggested to counter the self-weight of the top platen and eliminate any bedding movement.

Attention was specially made in erecting the column, to ensure the structure is vertically upright to avoid eccentric loading. Protective metal scaffolding was constructed around the specimen for safety. The two ends of the column were attached to a specially designed metal platform, which allowed the passage of fibre optic cables.

Before attaching the column to the metal platform, fixing clamps were removed. The slippage of fibre optic cables due to this removal was recorded by taking baseline measurements before and after the event.

Two LVDTs were installed at the middle at two adjacent sides of the specimen to detect any differential movement or beddings. This serves as an independent external displacement measurement of the structure. VWSG cables were connected to the read-out box whilst the spliced optical fibres were connected to the YOKOGAWA AQ8603 Optical Fibre Strain

Analyser with an extension cable of 50 m joined at one of the ends of optical fibre. This was adopted to minimise the connection end effects.

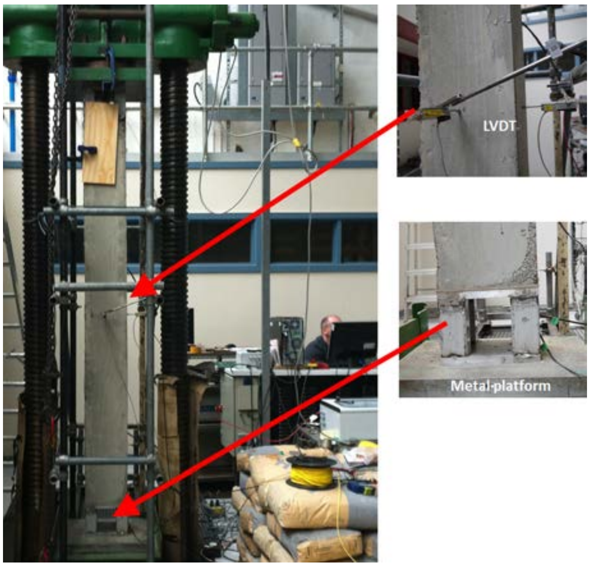

Figure 5.1 Experiment configuration for compression test

5.1.2 Procedures

Loading and re-loading cycles were introduced into the sprayed concrete column. There were a total of 15 load steps which consisted of 2 sets of loading and unloading. The first loading was 100 kN and was increased to 250 kN, 500 kN, 750 kN and 1055 kN (when the metal platform failed). Then the load decreased following the same load step to 250 kN. These procedures were repeated once and the final reading was taken at 57 kN.

VWSG measurements were taken every one minute starting before the application of pre-load. After the pre-load that stabilized the specimen, three BOTDR baseline strain measurements were taken to minimize test errors.

At each load step, three strain measurements were taken. Only two were made in later load steps due to time constraint. The strains in BOTDR average every 1m along the column length, 75 mm away from the surface. Measurement was conducted using a sampling rate of n = 15, frequency sweep of 10 MHz and a distance resolution of 10 cm. Using this setup, the acquisition time for each BOTDR measurement is approximately eight minutes.

5.1.3 Failure observation

The initial maximum load planned was 2200 kN (60% of the strength), however the supporting metal platform buckled at a load significantly below the strength of the concrete at 1100 kN. The bending of metal plate caused local failure of concrete at the corners as shown in Figure 5.2. For safety reason, the specimen was unloaded and it was decided that a maximum load of 1055 kN should not be exceeded for the remainder of the test.

Figure 5.2 Local failure at the corners of the specimen, with the base plate buckled.

5.2 Bending test

5.2.1 Set up

A mechanical screw jack was used to apply load for the bending test. A spreader beam on sliders was used to transfer the load at two points, 0.85 m from each ends of the beam, as illustrated in Figure 5.3.

Special attention was taken for turning the concrete beam over to rest on the Teflon® sheet pair to avoid damage. The adjustment of the beam was made using dental plaster pastes applied at the supports and the loading points.

Three LVDTs were installed at the opposite sides of the point loads and at the middle of the sprayed concrete beam to monitor deflections. Four VWSG cables were connected to the read-out box whilst fibre optic cables were connected to BOTDR without extension cable because the beam itself was long enough to minimise the effect of error. In addition, DEMEC gauges were used at five locations as shown in Figure 3.7 as additional backup device for surface strain measurements.

5.2.2 Procedure

Since the tensile strength of SFRC was small, the original design load step was 0.5 kN. However due to the difficulties in adjusting the load by the jack, the actual load steps were 0.8 kN, 1.07 kN, 1.5 kN, 1.8 kN, 2.0 kN, 2.4 kN, 3,0 kN, 3.5 kN, 4.1 kN, 4.5 kN, 5 kN, 5.6 kN, 6.0 kN, 6.4 kN and the concrete failed at 6.5 kN.

Similar to compression test, VWSG measurements were taken every one minute from the start of test. Before the first loading, three BOTDR baseline strain measurements were taken. Two strain measurements were then taken for each load step and at the end of the test. They were conducted again using a sampling rate of a sampling rate of n = 15, frequency sweep of 10 MHz and a distance resolution of 10 cm. The acquisition time for each BOTDR measurement is approximately eight minutes.

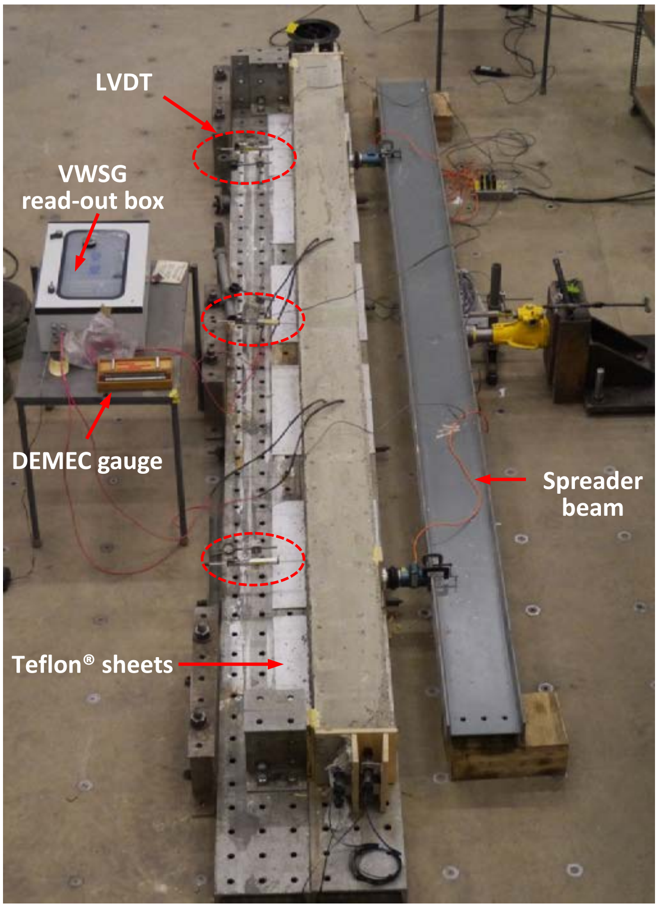

Figure 5.3 Experimental configuration for four-point bending test

5.2.3 Crack observation

A bending crack appeared at 2.85 m from the left. It was 1m away from one of the supports, where one set of VWSGs and a guiding steel bar were located. It was observed that an initial crack was formed at this location before the test (Figure 5.4). The steel bar, used to support the formwork, and the VWSG may have caused some localised weaknesses in the concrete (Figure 5.5). Transportation might also have caused the crack. The lack of steel fibres at this location due to uneven distribution could also explain the occurrence of failure.

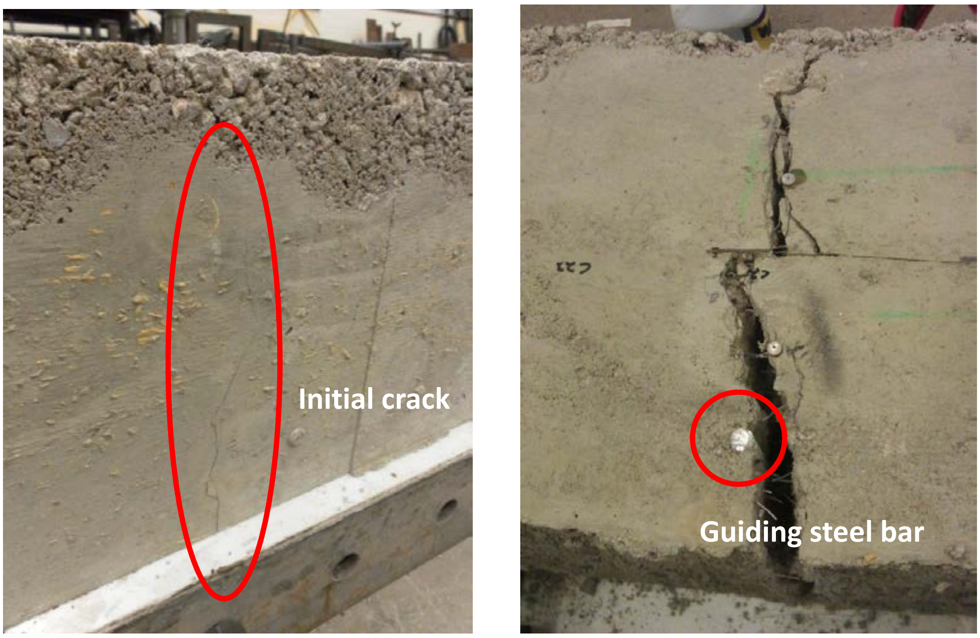

Figure 5.4 Crack (Left: before test, Right: after test)

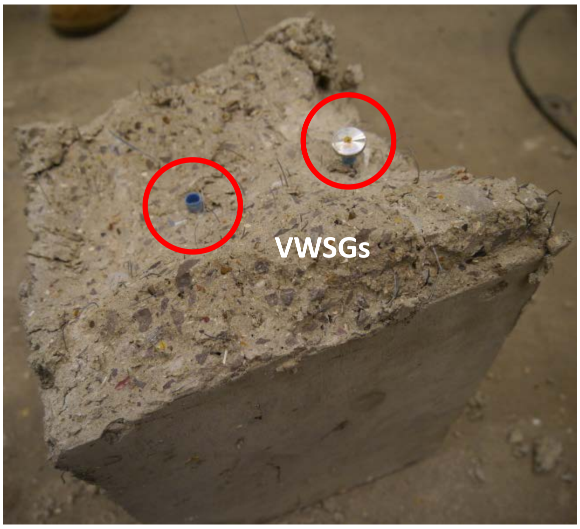

Figure 5.5 Crack surface with VWSGs clearly visible

5.2.4 Teflon® sheets revalidation

Teflon® sheets pair moved for a significant amount in the bending test (Figure 5.6), it is confirmed that Teflon® facilitated the movement of concrete beam. A revalidation test on Teflon® sheets was carried out after the bending test. The friction coefficient was evaluated to be 0.098, which was similar to the initial estimation.

Figure 5.6 The movement of Teflon® sheets after bending test

5.3 Data Processing

5.3.1 BOTDR data

BOTDR produces graphs with obvious changes in strains which are associated with clamping locations along the specimen. This is emphasized in Figure 5.7 and Figure 5.8 in red circles. In Figure 5.8, the two peaks of different magnitudes show that the pretensions imposed in the two fibre optic cables in the concrete beam were different.

The change in strain is calculated by removing average baseline measurements from the average strains measured at specific load, which is illustrated in Figure 5.9. The power of signal was in the range of 86 dB – 87 dB in compression test and 80 dB in bending test. According to the BOTDR manual, the accuracy is approximately between ±30 με and ±40 με.

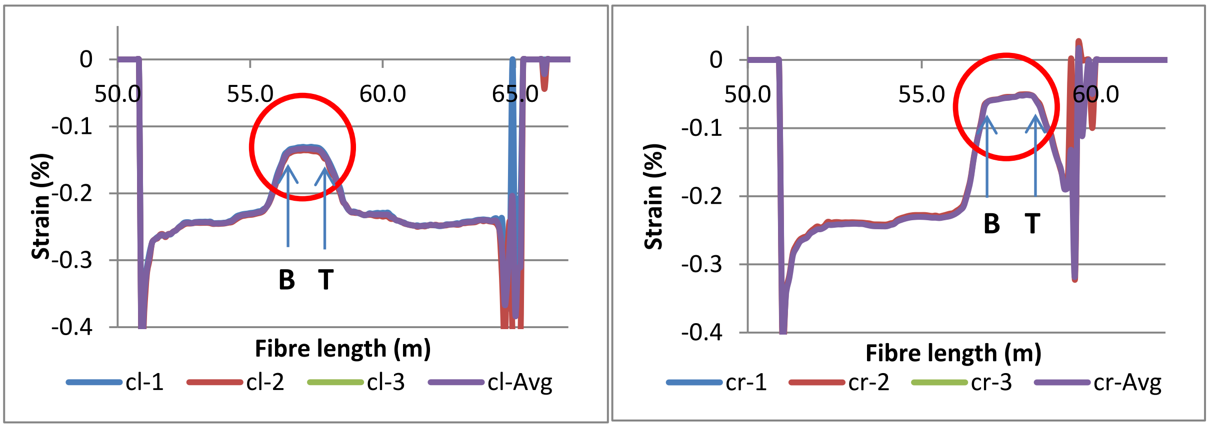

Figure 5.7 BOTDR in compression test at first increment

(Left: left optical fibre, Right: right optical fibre, where B= bottom of the column, T= top of the column)

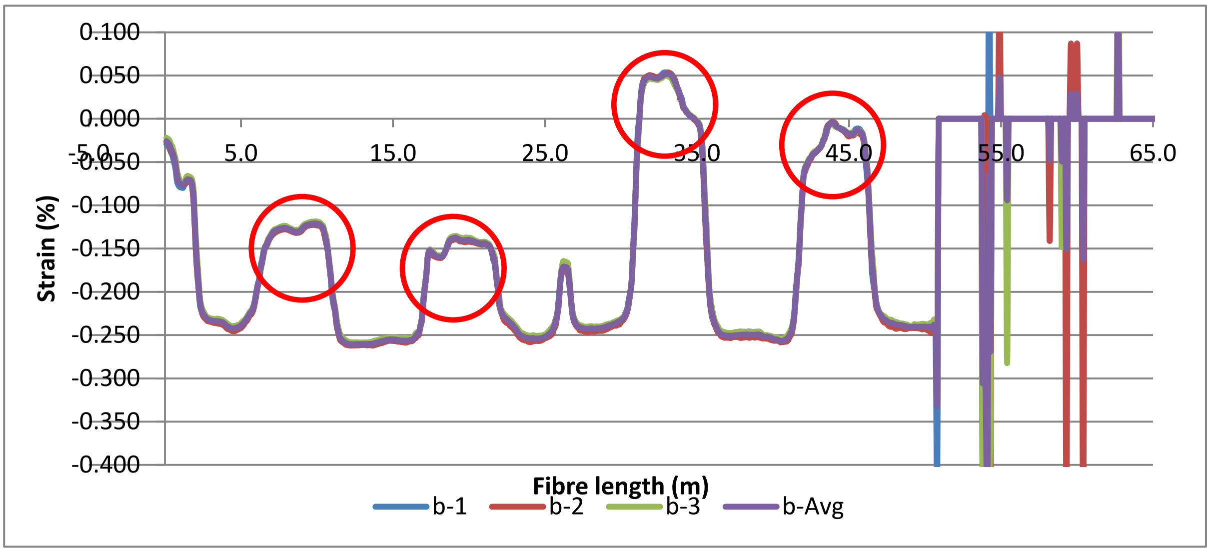

Figure 5.8 BOTDR reading in bending test at first increment

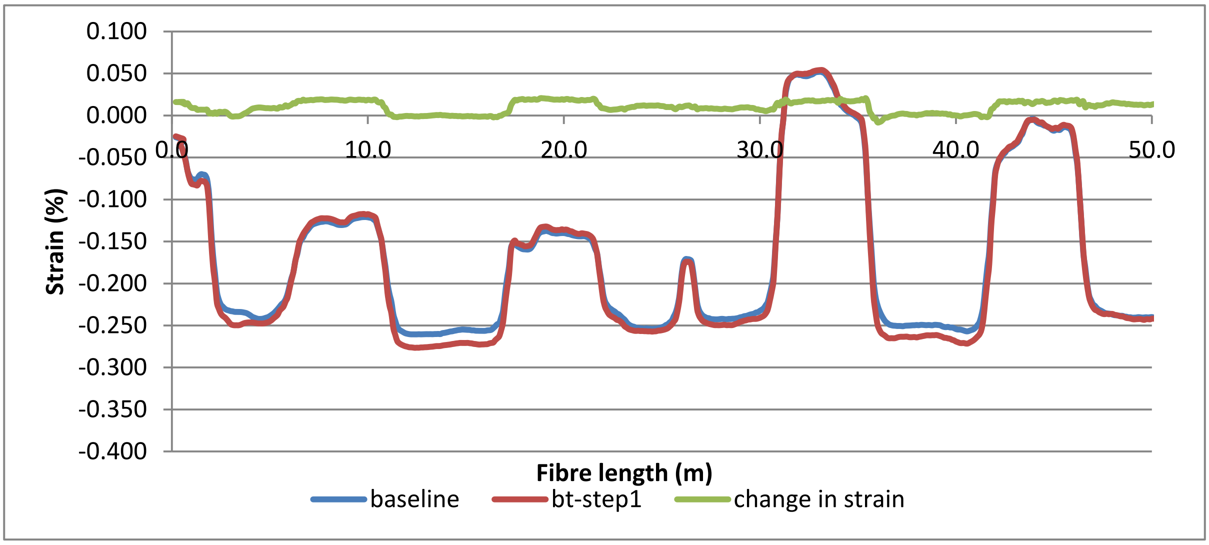

Figure 5.9 Change in strain in bending test at first increment

5.3.2 VWSG data

All data measured were corrected by eliminating the baseline measurements taken before the test. It is expected that the VWSGs originally over-register the strain, due to a small reduction in length of the vibrating wire caused by clamping. This effect is removed by applying a batch gage factor (B) supplied with each box of gauges. For the strain gauges used in experiment, the batch gauges factor is 0.975.

The apparent strain is calculated by:

$$\mu_{apparent} = B(R_1 - R_0) \qquad (5\text{-}1)$$

Where $\mathrm{R}_1 = \text{final strain reading}$

$\mathrm{R}_0 = \text{intial strain reading}$

$\mathrm{B} = \text{batch gauge factor}$

5.3.3 Temperature compensation

Both Optical fibres and VWSG are sensitive to temperature changes. The temperature measured in VWSG was used in modifying the strain data correspondingly.

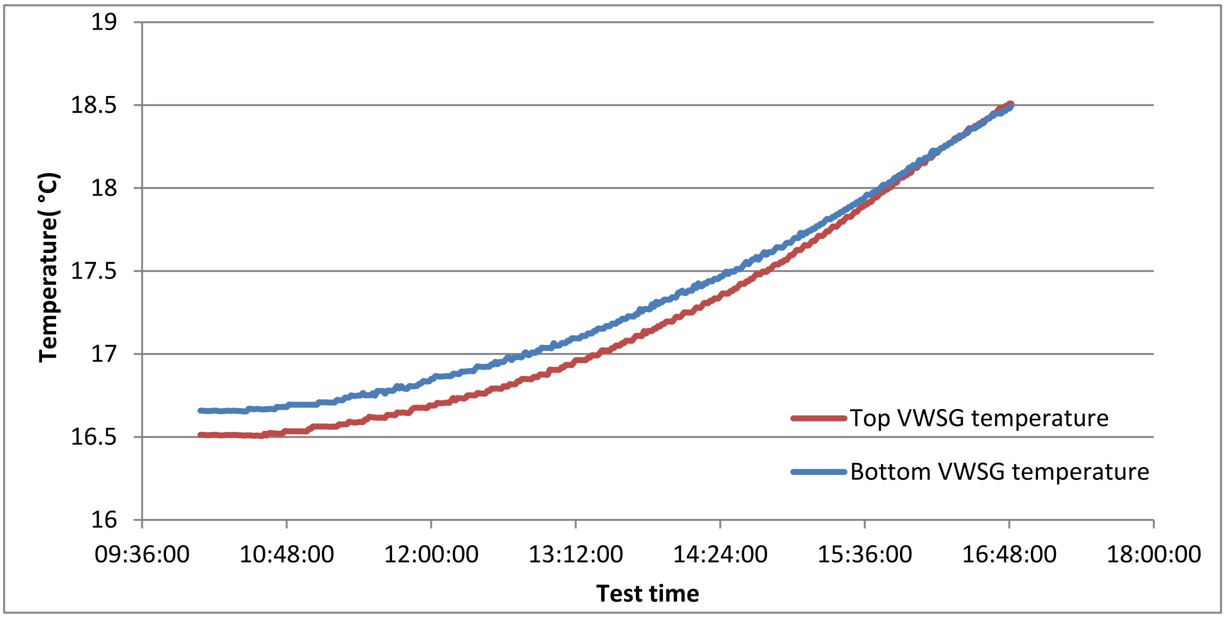

Figure 5.10 Temperature change in VWSG during compression test

The temperature change was 2 °C during compression test and small increase during bending test, there were minor difference between the temperatures read at different VWSGs.

This temperature change is not caused by the environment because the tests were taken in a laboratory with reasonably constant temperature. It is believed that this change may be caused by the VWSG itself due to heat generated by the electricity in long term usage. Therefore the general temperature of the concrete is considered to be constant in both tests. BOTDR readings should not take into the account of temperature change for analysis.

The true load related strain after temperature compensation is calculated according to the manual of Model 4200 strain gauges. The influence of temperature on strain measurement is insignificant.

$$\mu_{load} = (R_1 - R_0)\mathrm{B} + (T_1 - T_0)(C_1 - C_2) \qquad (5\text{-}2)$$

Where $\mathrm{T}_1 = \text{final temperature}$

$\mathrm{T}_0 = \text{initial temperature}$

$\mathrm{C}_1 = \text{coefficient of expansion of steel} = 12.2\mu\varepsilon/(°\mathrm{C})$

$\mathrm{C}_2 = \text{coefficient of expansion of concrete} = 10\mu\varepsilon/°\mathrm{C}$

5.3.4 Reasonable data read from BOTDR

The strains read from the BOTDR at both ends of the column were not accurate due to the characteristic of BOTDR. Since it averages strain every 1 m, the strains outside the column which was zero were included in producing strain at the ends of the column, hence the strain appeared to be gradually decreasing towards the ends. Only data reasonably away from the ends should be considered for analysis, ranging from 0.5 m to 1.8 m from the bottom. In Figure 5.11, the average BOTDR measurements produced by averaging strains from the left and right optical fibres in the column are presented.

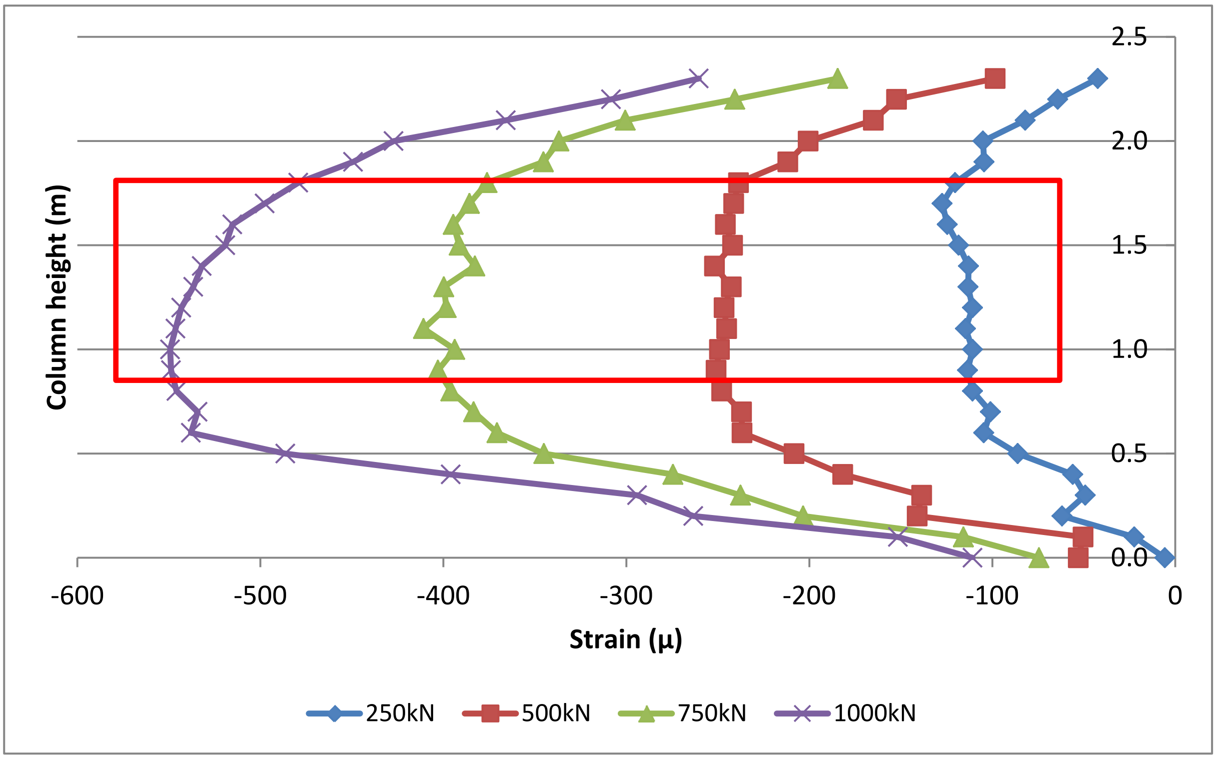

Figure 5.11 Strain distribution on the column at different loading (Before the metal platform collapse)

5.3.5 LVDT stress-strain curve adjustment

The metal platform that supports the column during compression failed at approximately 30% of the strength of the concrete. Since the LVDT measured the total displacement of the compressed concrete and metal collapse, it has to be adjusted to identify the actual deformation of concrete. This is done by assuming the strain at load 1055 kN, with a corresponding stress of 16.88 MPa (after the metal platform failed), followed the linear elastic path, which shifts the curve towards zero.

The loop generated by the effects of unloading and reloading suggests the concrete was stiffer after the first loading, which is very unlikely. This may be caused by the failure of the metal platform. This increase in stiffness was only calculated from the LVDT data which further supports the argument that it is not related to change of concrete properties.

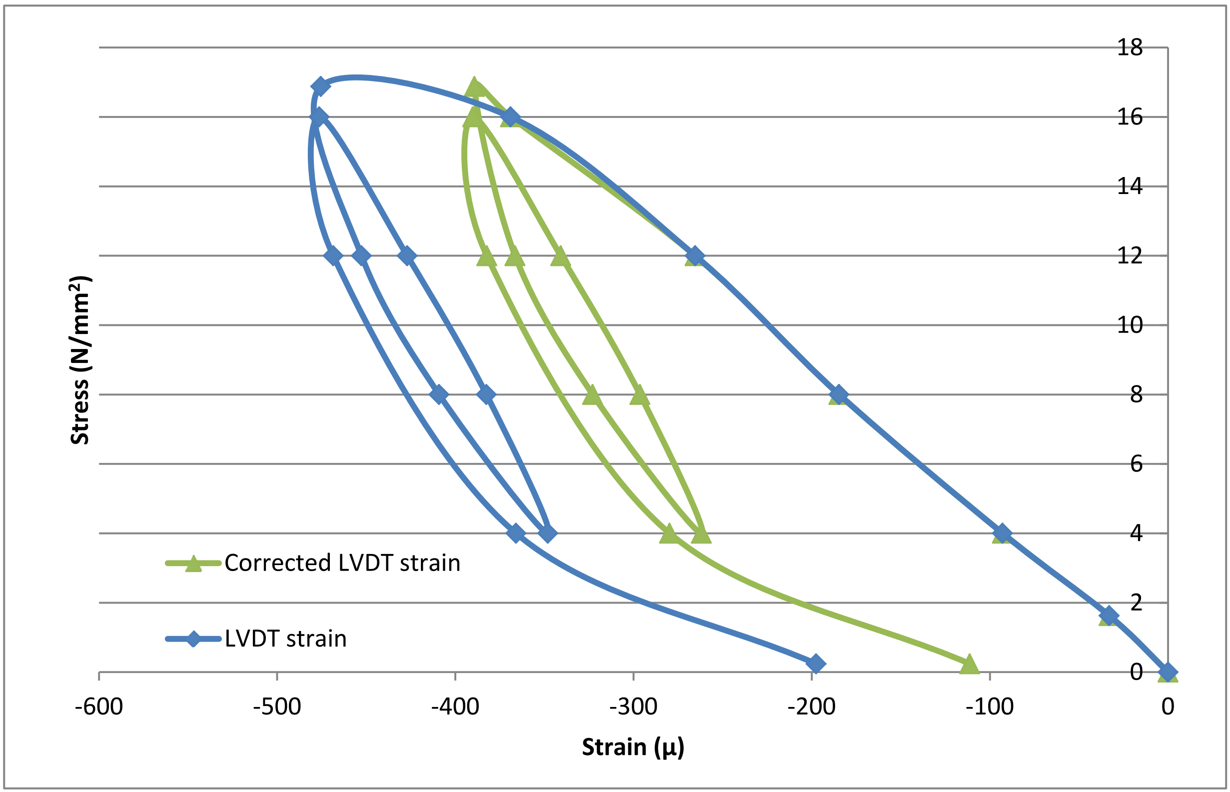

Figure 5.12 LVDT stress strain curve adjustment

5.3.6 Comparing curvature

In the bending test, a full optical fibre with no breakage gives distinctive indications on location of beam due to change in strain pattern. However the distribution and the amount of induced strains are not as obvious and easy to understand.

In Figure 5.13, where fibres 2 & 3 should experience compression and fibres 1 & 4 should experience tension, they did not reflect this behaviour in first increment of load shown in Figure 5.14, instead all seem to have experienced tensile stresses. This shifting can be caused by a number of factors, including temperature change and slippage that cannot be easily quantified. It is also noted that comparing with the accuracy of BOTDR (±30 με), the strain induced is insignificant to be justified. Hence a more reasonable element to verify readings between BOTDR and VWSGs would be curvature, which is calculated by:

$$k = \frac{difference\ in\ strain\ in\ cross\ sectional\ area}{distance\ \ between\ measurements}$$

(5-3)

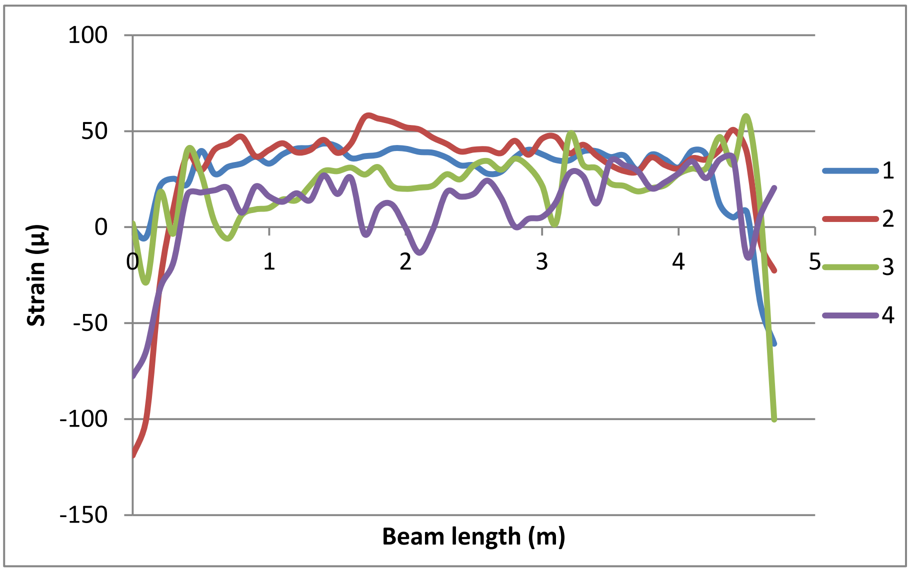

Figure 5.14 Change in strain distribution along the beams in first loading

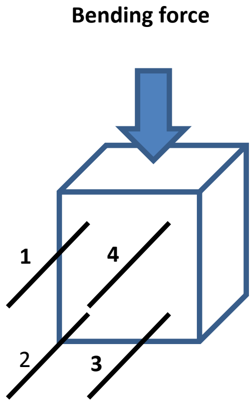

Figure 5.13 Optical fibre configuration

6 Results & Observations

6.1 Compression test

6.1.1 Slippage from pretension

The pretension of fibre optic cables in the column was approximately 3000 µε (0.3 %). Comparison has been made between readings taken before and after the removal of pre-tensioning clamps. The slippage was in the range of 300 µε and 350 µε which is considered to be reasonable (~10 % of pretension). Clamps are not removed from the beam hence no slippage was observed. It was also proved that the slippage during the compression test was very small, by comparing the initial reading to the final reading after the test had finished under no loading, which was +30 µε. This is within the accuracy of the BOTDR.

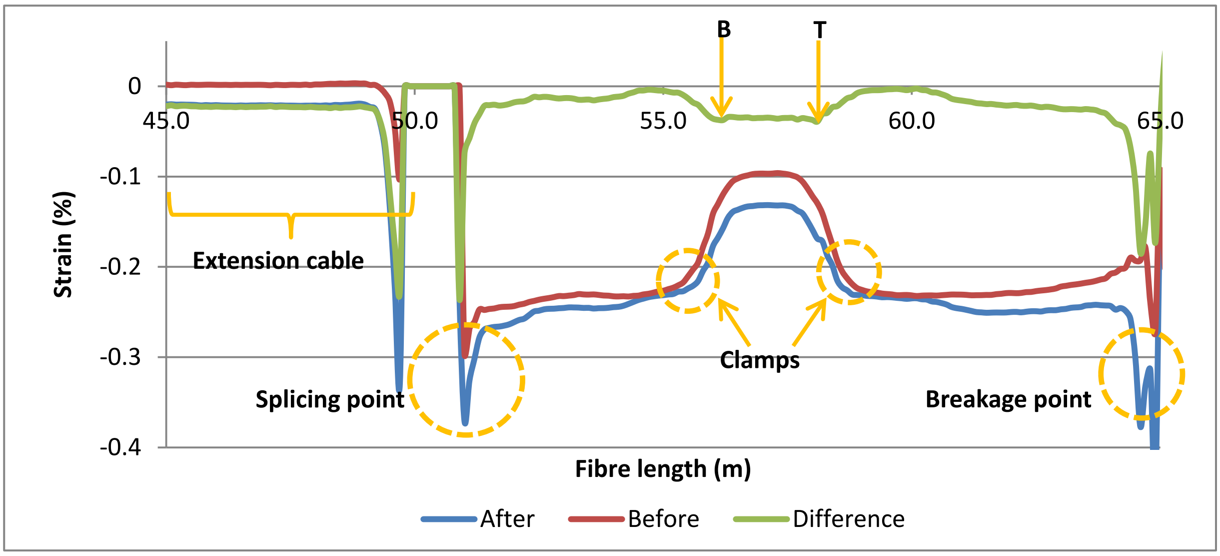

Figure 6.1 Comparison of strain measured before and after the removal of clamps on the left fibre.

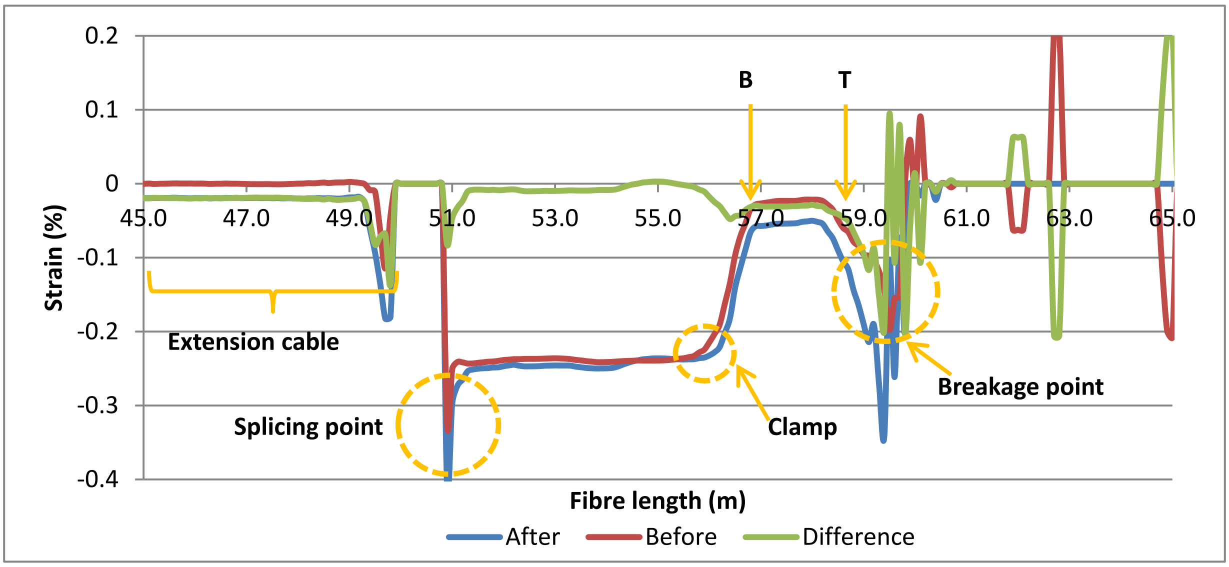

Figure 6.2 Comparison of strain measured before and after the removal of clamps on the right fibre.

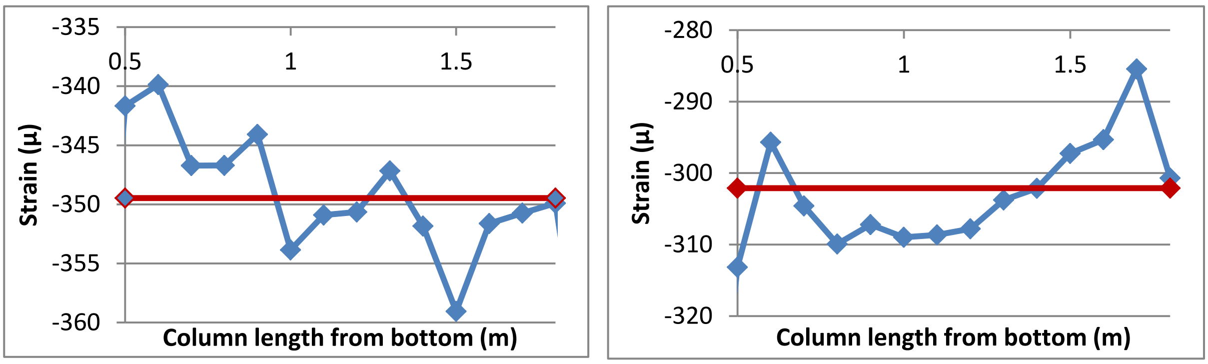

Figure 6.3 Change in strain due to clamps removal (Left: left fibre cable, Right: right fibre cable)

6.1.2 Strain distribution

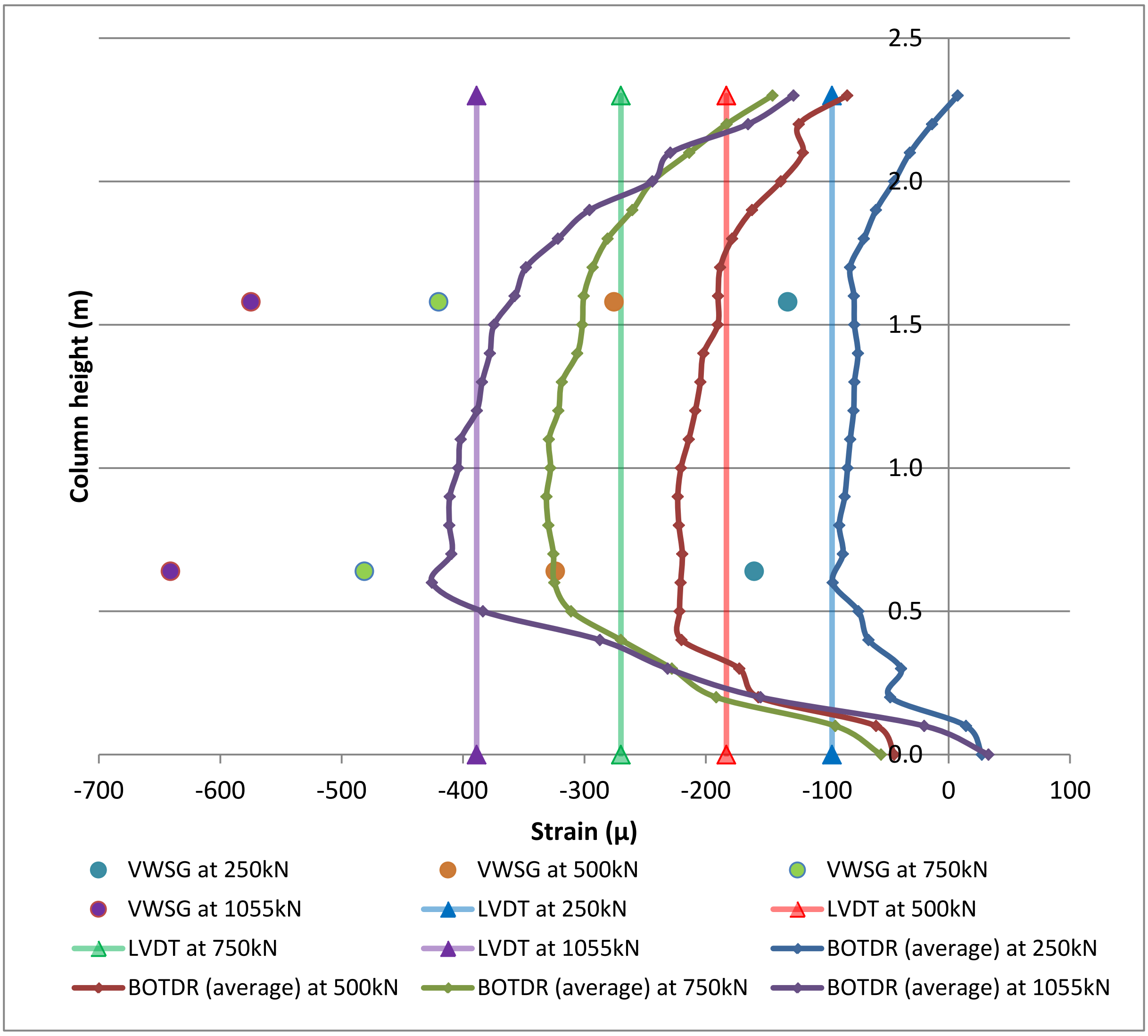

Figure 6.4 Strain distribution along the column before metal collapsed

It is observed that the average BOTDR readings match with the LVDT readings, while VWSG measurements are generally higher in compression.

There are four possibilities. Firstly, VWSG may be affected by temperature changes; however this effect is very small as discussed. Secondly, LVDT measurements may be influenced by the bending of metal platforms even before the collapse, but the inaccuracy induced should be minimal because of the elastic behaviour and high stiffness of steel. Thirdly, there could be slippage in fibre optics cables, in which the compressive stress of the concrete could not be fully transmitted to the fibre. With the fixing clamps removed and a weak bonding between fibre and concrete assumed, the fibres had a tendency to contract more than concrete under compression, hence were overestimating the compressive strain. This is unlikely because it has been proved that slippage during compression was small. Lastly, the VWSG may be "corrected" with a bad calibration factor supplied with the batch of gauges that is not applicable to those particular gauges used. This has the highest possibility and would be further explored in the bending test results.

6.1.3 Young's Modulus

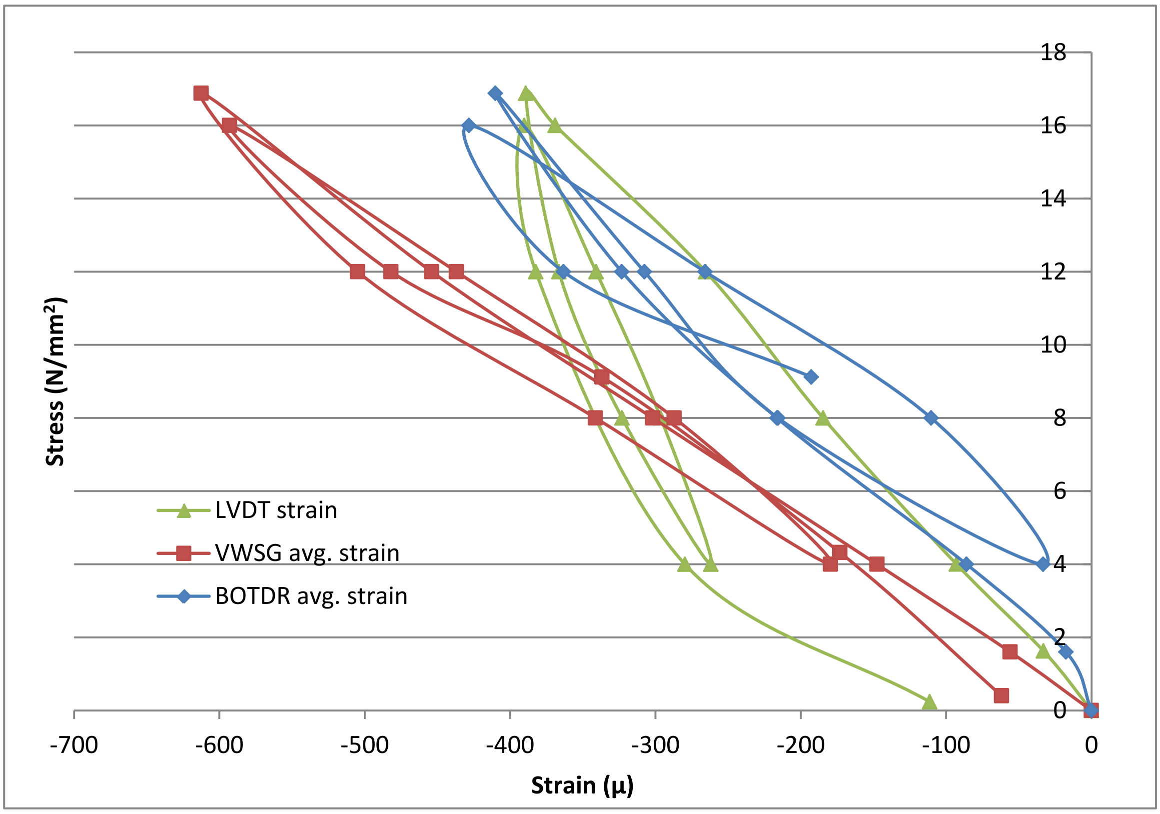

Figure 6.5 stress-strain curves

It is shown that stress-strain curve of BOTDR follows the path of LVDT, while the strains measured by VWSG are approximately 1.5 times larger than BOTDR. This follows the discussion in the previous section that VWSG may have over-estimated the strains.

It is observed that the stress-strain curves produced by the BOTDR and VWSG are relatively linear, which posts a possibility that there may be calibration problem with the VWSG readings. By calculating the gradient of best-fit lines for each of the curves, the Young's modulus of concrete predicted by BOTDR, LVDT and VWSG are 41.2 GPa, 43.4 GPa and 27.8 GPa respectively. BOTDR and LVDT predictions agree very well with CEB-FIP Model Code 1990 prediction (38.9 GPa) while VWSG prediction does not match with any of the theoretical predictions.

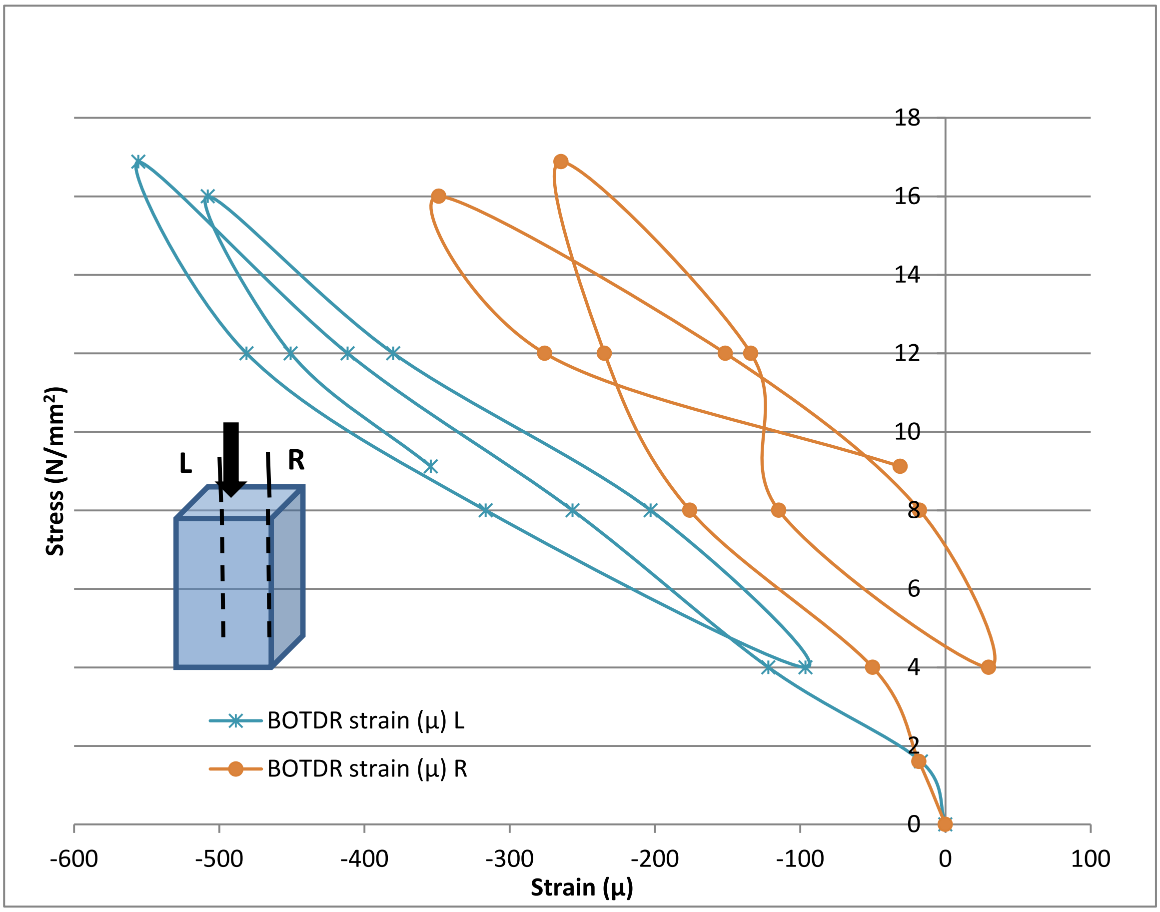

Figure 6.6 stress strain curve produced by BOTDR (Left and Right)

It is an interesting point to note the difference of strain measured by the optical fibres in the left and right of column. In uniaxial compression test, it is assumed that the strain is the same within the column. However, Figure 6.6 suggested eccentric loading had taken place.

The left fibre recorded higher compressive strains than the right fibre, demonstrating the point of eccentricity is closer to the left of the column. This can be further established with equations. The moment created by compressive load is

$$\mathrm{M} = \mathrm{N} \cdot \mathrm{e} \tag{6-1}$$

where N is the compressive load and e is the eccentricity.

The stresses at left and right of the column are:

$$\sigma = \frac{N}{A} \pm \frac{M}{Z} \tag{6-2}$$

where A is the cross-sectional area and Z is the modulus of section ($bh^2/6$)

$$\sigma_{left} = \frac{N}{A} + \frac{M}{Z} = \mathrm{N}\left(\frac{1}{A} + \frac{e}{Z}\right) \tag{6-3}$$

$$\sigma_{right} = \frac{N}{A} - \frac{M}{Z} = \mathrm{N}\left(\frac{1}{A} - \frac{e}{Z}\right) \tag{6-4}$$

And hence,

$$\sigma_{left} - \sigma_{right} = \frac{2Ne}{Z} \tag{6-5}$$

$$\varepsilon_{left} - \varepsilon_{right} = \frac{2N \cdot e}{Z \cdot E} = \sigma_{overall} \cdot \frac{2 \cdot A \cdot e}{Z \cdot E} \tag{6-6}$$

Where A is the cross sectional area and E is the Young’s Modulus.

Assuming E = 34000 MPa, using strains at 750 kN in first loading, the eccentricity is very small which is approximately 0.01 mm.

After the metal platform collapses, the metal plate deformed irregularly and eccentricity may change unpredictably. This explains the non-uniform change in strain due to unloading and reloading especially in the right optical fibre.

6.1.4 Cyclic loading effect

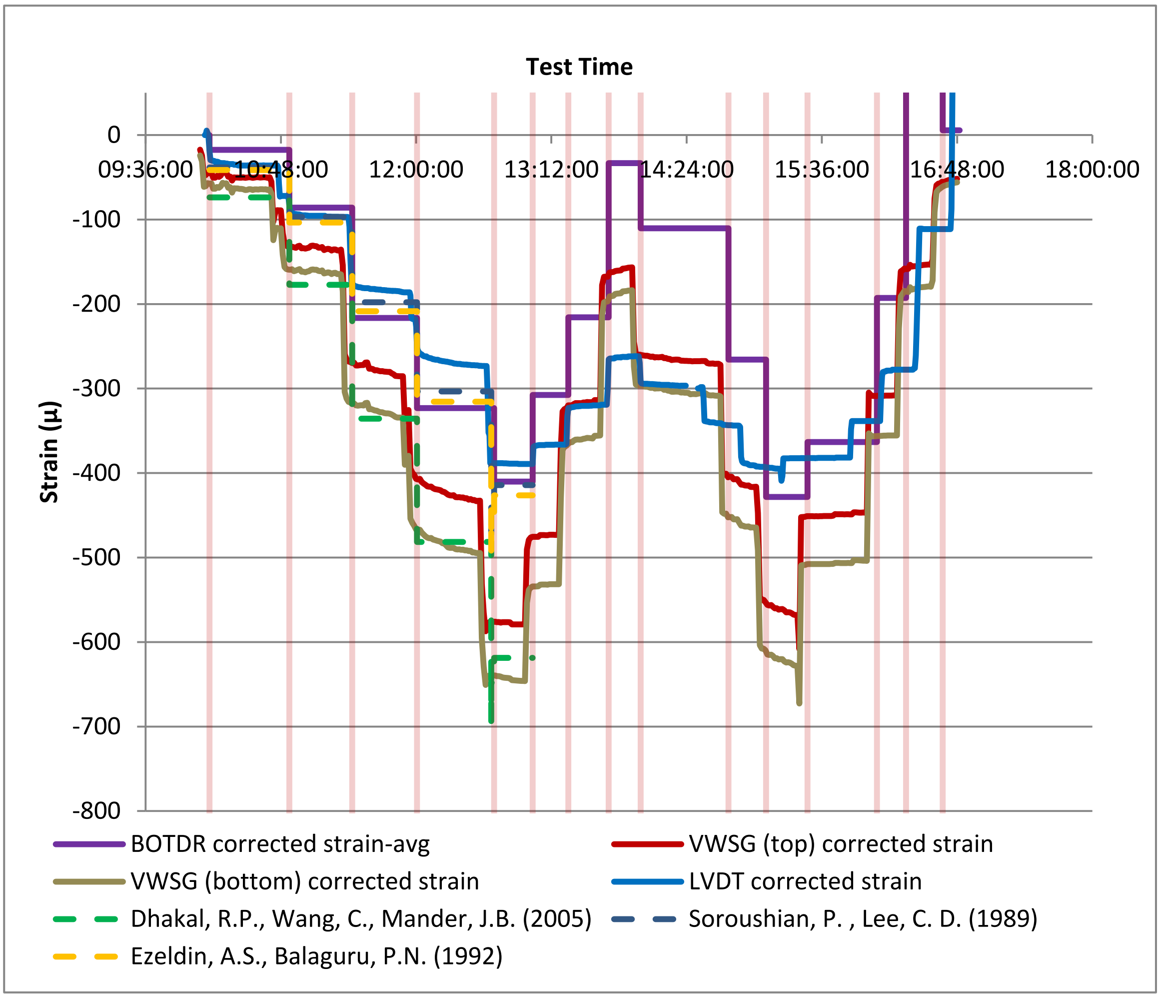

Figure 6.7 Change in strain against time

The strain changes according to loading increments, which are shown as vertical red lines. However an observation is made that the strains induced in the concrete at the same loading were different in loading path and unloading path.

The obvious example is the strains recorded after and before hitting the maximum load (at 750 kN), the compressive strain appears to be higher in unloading path. Creep and relaxation effects are unlikely, as they need a relatively longer time to have any influence. It is believed that this phenomenon is caused by the nature of sprayed concrete where non-linearity is expected in that range of loading. Strain followed a convex loop when unloaded.

6.2 Four point bending test

6.2.1 VWSG and DEMEC gauges measurements

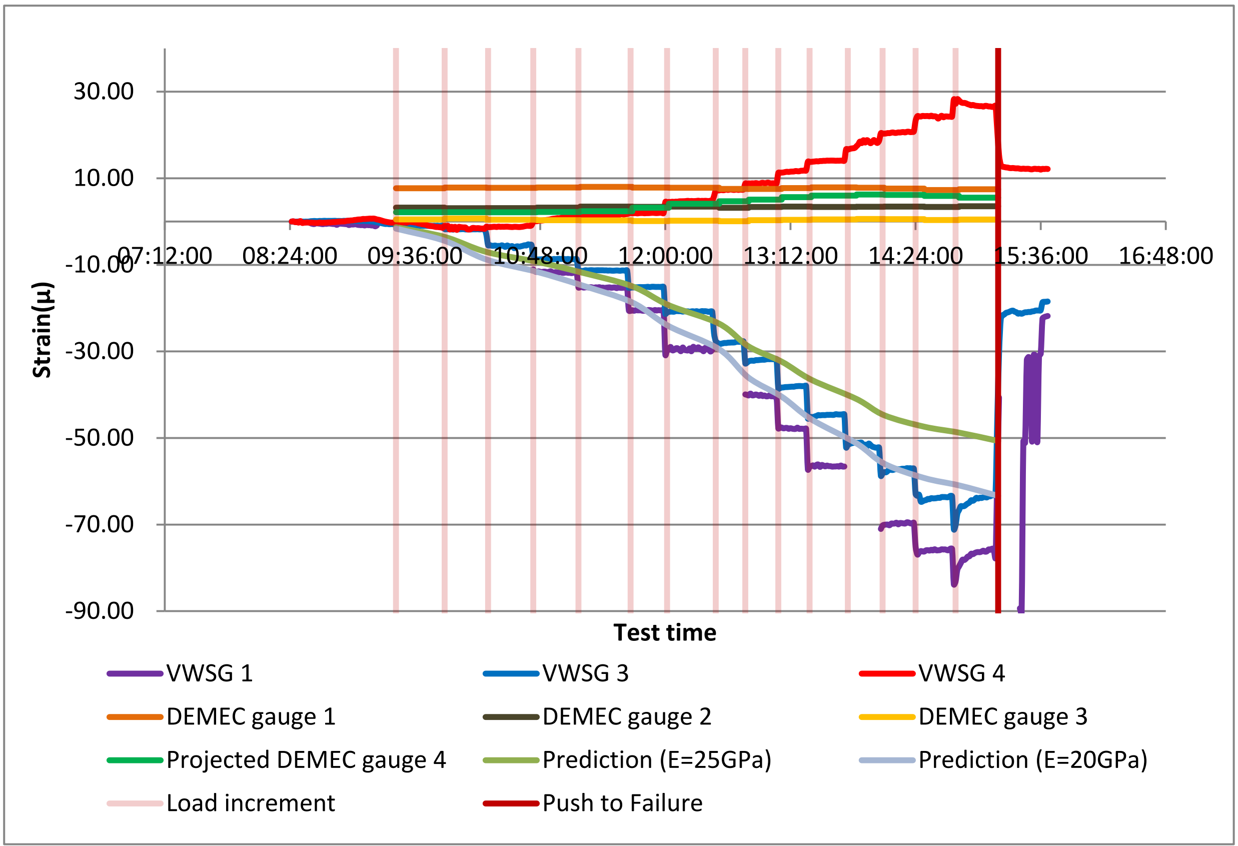

Figure 6.8 VWSG and DEMEC gauges readings

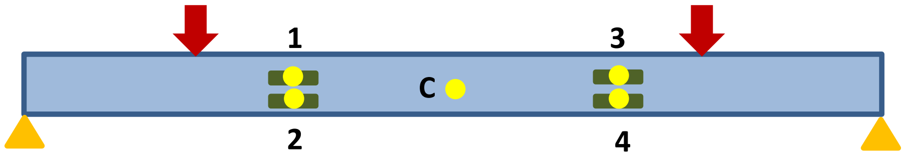

Figure 6.9 VWSG and DEMEC gauges layout (Green = VWSG, Yellow = DEMEC gauges)

The DEMEC gauges did not work well in bending test. The strains induced during the bending test may have been too small for the Deme gauges to measure. With DEMEC gauges, VWSG and prediction strain curves plotted in Figure 6.8, considering the loading before crack (first few steps), the concrete is estimated to have a stiffness of 20-25 GPa which is comparatively small to prediction. Hence, it is again confirmed that VWSG over-estimated the strains.

6.2.2 BOTDR Curvature

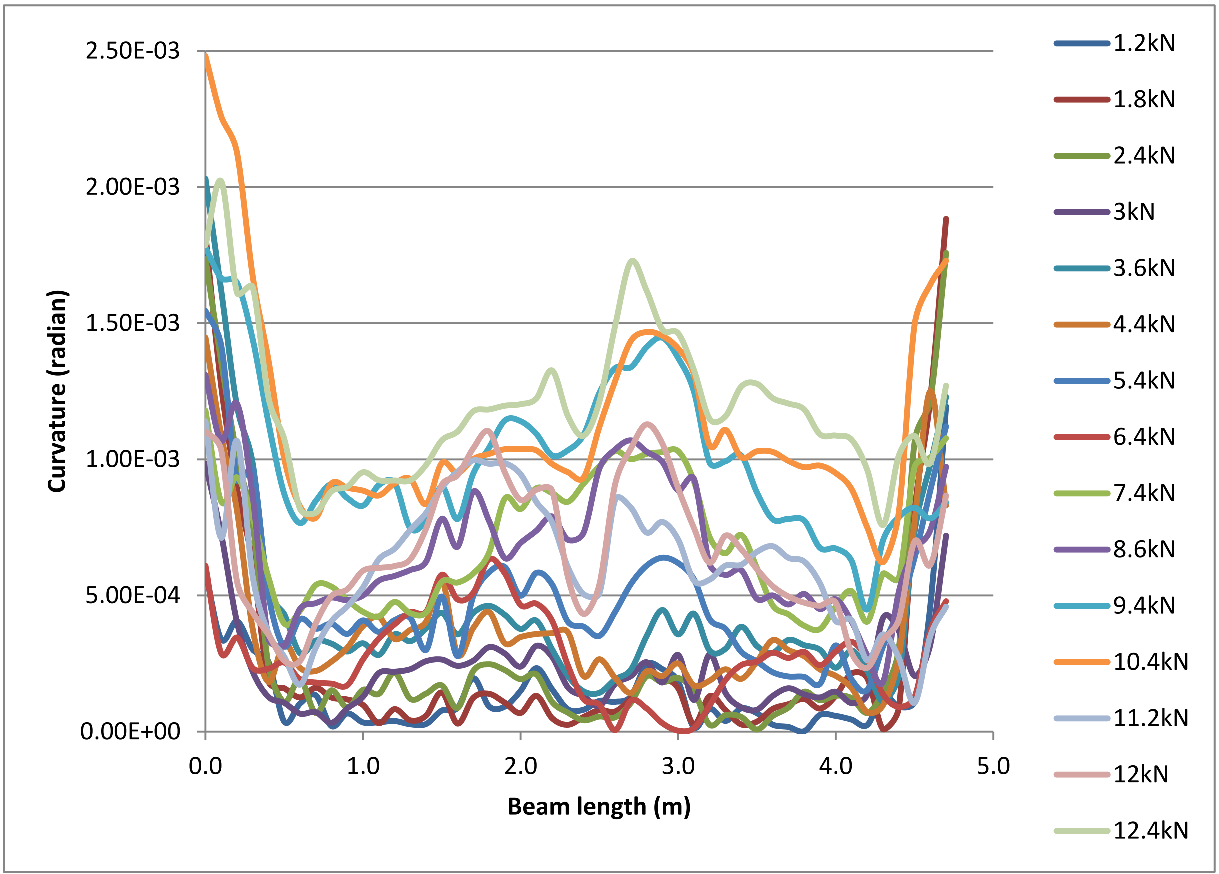

Figure 6.10 Curvature predicted by BOTDR at different loading

Figure 6.7 shows a steady increase in curvature with increasing load until reaching a total load of 12.4 kN where concrete started to fail. A significant peak arises at 2.84 m where the crack was formed and becomes more obvious from a total load of 7.4 kN onwards.

By eliminating the effect of crack propagation, the BOTDR illustrates a rather constant curvature between 0.85 m and 3.85 m, as expected.

6.2.3 Curvature comparison

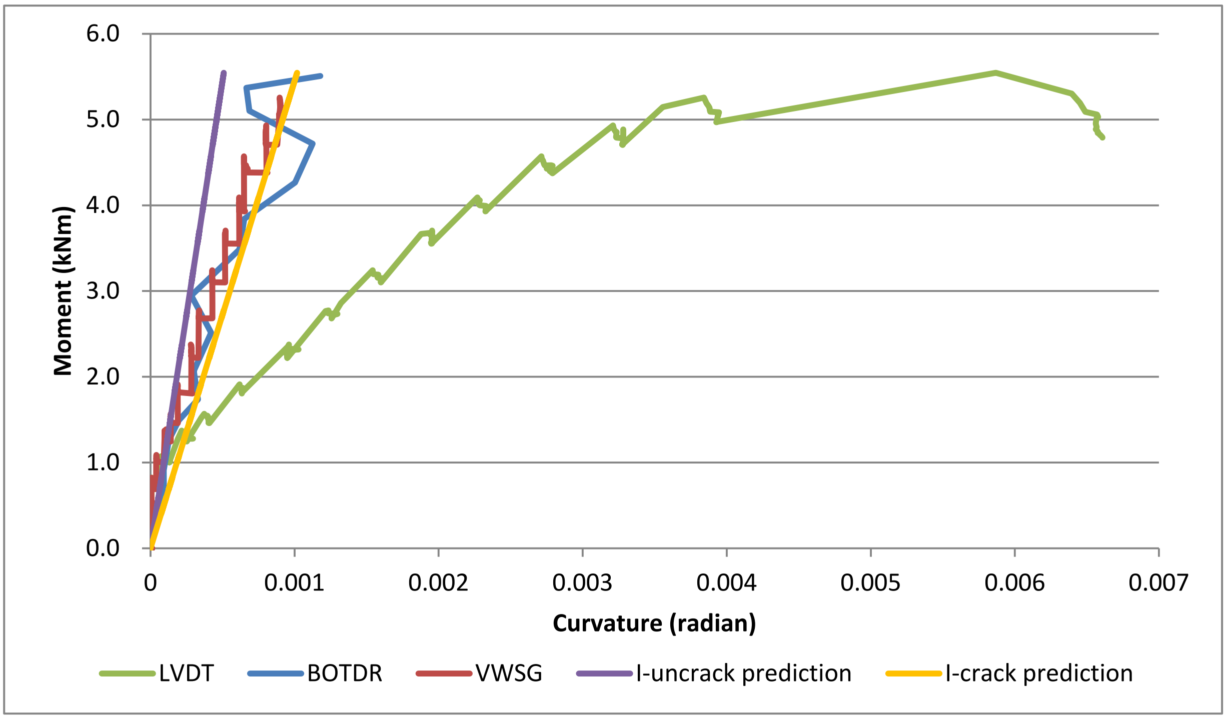

Figure 6.11 Comparison of average curvature between two point loads

The average curvature between point loads is calculated from BOTDR, VWSG and DEMEC gauges measurements. Curvature due to crack is removed in averaging the curvature from BOTDR for consistency. The predicted values are calculated considering an uncrack section ($I_{uncrack}$) and a crack section (I_{crack}), using $M = EI\phi$ with E equals to 39.4 GPa. For the crack section, it is assumed that the beam was purely sustained by the concrete in tension.

In Figure 6.10, VWSG shows a relatively constant increasing trend, which is similar to BOTDR. This contradicts with the results obtained in the compression test. BOTDR predicts wrongly with data relatively scattered, due to the significant error in the curvature calculation (±600 $\mu\varepsilon$ /m, given that the distance between two gauges is 0.1 m).

LVDT, which measured external displacement, is sensitive to the appearance of crack. This is illustrated by the rapid change in gradient at 1 kNm. With no reinforcement, the transition from an uncrack section to a crack section is gradual. This is demonstrated by the VWSG and DEMEC gauges, where their data slowly shift from $I_{uncrack}$ predictions to I_{crack} predictions.

6.3 Findings Summary

Table 6-1 Summary table of stiffness

	Compression test (GPa)	Bending test (GPa)
BOTDR	41.2	23
VWSG	27.8	23
LVDT	43.4	11*
Predictions	40.2	39.4

*Using M=Eiϕ, by ratio of LVDT to VWSG and assuming Icrack.

By comparing the stiffness predictions, it is clear that from the compression test, BOTDR and LVDT agreed with the prediction whilst VWSG over-estimated the strains possibly due to the bad calibration factor supplied.

In the bending test, it is again confirmed that VWSG overestimated the strains and gives a lower Young's modulus than predicted. BOTDR underestimates the Young's modulus in this context because of the expansion of error. A very low modulus is calculated from LVDT, which may be caused by the decrease in stiffness due to cracking. Further investigations are needed to be carried out to confirm these findings.

7. Conclusions

This research aims at examining the accuracy, practicality and robustness of BOTDR technology, in comparison with conventional VWSG when employed in sprayed concrete applications.

In term of accuracy, BOTDR measurements were promising in both the compression and bending tests. Its results were verified by external displacement readings of the LVDT and stiffness predictions. VWSG were considered to have overestimated the strain measurements, as these will depend on the calibration factor. BOTDR revealed more information regarding the behaviour of the structure and was able to pinpoint a crack at a short period of time. This is critical for the development of smart structures that respond to problems quickly.

Fujikura reinforced ribbon cable provides good protection for optical fibres to perform properly under harsh installation environments and good bonding with sprayed concrete without the need to attach the cables to the reinforcing bars. Although a kink caused disturbance of strain measurements in the column, these information were recovered by accessing through the other end of the fibre. One out of six vibrating wire strain gauges was damaged before testing at CUED and its measurements can never be retrieved. This gives an insight into the reliability of the VWSG when used in real life scenarios.

Special care is required in handling optical fibres. Splicing is one of the challenging skills that require high precision. It is less user-friendly and could be impractical in constructions situations especially when lighting is insufficient and time is a major constraint. However, it is foreseeable that with a splicing technique that require less labour work and time, distributed optical sensing could be a highly viable monitoring tools in the civil engineering industry in the future. This is particularly true for harsh environments like sprayed concrete.

8 Bibliography

Barros, J. A. O., Figueiras, J. A. "Flexural behavior of steel fiber reinforced concrete: Testing and Modeling." *Cement and Concrete Composites* Vol. 27, no. 4 (April 2005): 471 - 480.

Carreira, D. J. , Chu, K. M. "Stress-strain relationship for plain concrete in compression." *ACI J.*, 6 1985: 797 – 804.

Dhakal, R.P., Wang, C., Mander, J.B. "Behavior of steel fibre reinforced concrete in compression." *Nanjing:International Symposium on Innovation & Sustainability of Structures in Civil Engineering*, Nov 2005.

Ezeldin, A.S., Balaguru, P.N. "Normal and high strength fiber-reinforced concrete under compression." *Journal of Materials in Civil Engineering* (ASCE) Vol. 4, no. 4 (1992): 415 - 429.

Jo, B.W., Shon, Y.H., Kim, Y.J. "The Evalution Of Elastic Modulus for Steel Fiber Reinforced Concrete." (Russian Journal of Nondestructive Testing) Vol. 37, no. 2 (2001): 152-161.

Labib, W., Eden, N. "An Investigation into the use of fibres in concrete industrial ground-floor slabs." *3rd International Built a. Human Environment Research Week*, 2006.

MacGregor, J. G. , Wight, J. *Reinforced Concrete: Mechanics and Design.* Third Edition. Prentice-Hall, Inc., 1997.

Mohamad, H. *Distributed Optical Fibre Strain Sensing of Geotechnical Structures.* Cambridge: Department of Engineering, University of Cambridge, 2008.

Shende, A.E., Pande, A.M. "Experimental study and prediction of tensile strength for steel fiber reinforced concrete." *International Journal of Civil and Structural Engineering* Vol. 1, no. 4 (2011).

Soroushian, P. , Lee, C. D. "Constitutive modeling of steel fiber reinforced concrete under direct tension and compression." *Fibre reinforced cements and concretes, recent developments*, 1989: 363 – 375.

Appendix I-Risk Assessment Retrospective

The risk assessment submitted to the Safety Office at the start of the Michaelmas Term was constantly reviewed and revised throughout the course of this project. The hazards were correctly listed and the mitigation control measures suggested were carefully followed.

The initial risk assessment stated the rough ideas of the work involved in this project, including site work and experimental work. Risk assessments of similar projects were reviewed. As the research proceeded, planning and considerations became more detailed, hence a modification of the risk assessment was required to encounter these changes.

Two modifications were completed, only supplementary information were added, such as specification of concrete mix and Teflon® sheets, safety calculations of rig and supports. Risks were generally not underestimated at the beginning of the research.

The risk assessment is considered to be complete and relevant, the method of writing the initial risk assessment and the idea of reviewing it constantly are good practices that should be kept when working on other projects.